Low-Complexity Joint Power Allocation and Trajectory Design for UAV-Enabled Secure Communications with Power Splitting

Kaidi Xu, Ming-Min Zhao, *Member, IEEE,* Yunlong Cai, *Senior Member, IEEE,* and Lajos Hanzo *Fellow, IEEE*

***Abstract*—An unmanned aerial vehicle (UAV)-aided secure communication system is conceived and investigated, where the UAV transmits legitimate information to a ground user in the presence of an eavesdropper (Eve). To guarantee the security, the UAV employs a power splitting approach, where its transmit power can be divided into two parts for transmitting confidential messages and artificial noise (AN), respectively. We aim to maximize the average secrecy rate by jointly optimizing the UAVs trajectory, the transmit power levels and the corresponding power splitting ratios allocated to different time slots during the whole flight time, subject to both the maximum UAV speed constraint, the total mobility energy constraint, the total transmit power constraint, and other related constraints. To efficiently tackle this non-convex optimization problem, we propose an iterative algorithm by blending the benefits of the block coordinate descent (BCD) method, the concave-convex procedure (CCCP) and the alternating direction method of multipliers (ADMM). Specially, we show that the proposed algorithm exhibits very low computational complexity and each of its updating steps can be formulated in a nearly closed form. Besides, it can be easily extended to the case of three-dimensional (3D) trajectory design. Our simulation results validate the efficiency of the proposed algorithm.**

***Index Terms*—Physical layer security, UAV, artificial noise, trajectory design, power allocation.**

I. Introduction

Unmanned aerial vehicular (UAV) communications have recently attracted growing research interests in both academia and industry [1]–[9], given their unique benefits of prompt on-demand deployment, low latency as well as agility and flexibility. Since UAVs are generally expected to operate at a higher altitude than conventional cellular base stations (BSs), the line-of-sight (LoS) component dominates the air-to-ground/ground-to-air channels in many practical scenarios [10]. Hence UAV-aided LoS links tend to have better channel quality than typical terrestrial channels, which often suffer from severe fading and shadowing effects. However, unfortunately the UAV-aided LoS links suffer from an increased eavesdropping probability [11] due to the open broadcast nature of wireless channels. From this perspective, the LoS propagation of UAVs becomes a double-edged sword, since additionally the terrestrial communications are also potentially exposed to malicious UAVs. Therefore, the delicate handling of the underlying security issues holds the key to unlocking the potential of UAV-aided communications.

Recently, physical layer security has drawn significant attention in UAV-enabled communication systems as a promising technique of protecting legitimate transmissions against eavesdropping attacks and also as a complement of conventional encryption techniques [12], [13]. Focusing on resource allocation/management for secrecy communication performance maximization, a range of physical layer security (PLS) techniques have been considered in the literature, such as UAV-mounted BSs [14]–[18], UAV-enabled relaying [19] and UAV-assisted cooperative jamming [2], [20]–[24], etc. In particular, a single-UAV communication system was investigated in [14], where the UAV sends confidential information to a legitimate ground user (Bob) in the presence of a ground-based eavesdropper, and the secrecy rate is maximized by jointly allocating the UAV's transmit power and optimizing its flight trajectory. The authors of [15] have considered a scenario of multiple users and maximized the minimum secrecy rate for ensuring fairness among the users. By contrast, the authors of [16] considered coordinated multi-point (CoMP) reception of the legitimate users and three-dimensional (3D) trajectory optimization in the presence of multiple malicious eavesdroppers. In [17], the total transmit power of the UAV-mounted BS was minimized through joint beamforming optimization. As a further development, the authors of [19] studied the security problems of UAV-aided relaying systems and judiciously shared the transmit power between the source and the UAV.

Furthermore, in addition to exploiting the agile maneuverability of the UAVs for improving their secrecy performance, UAVs can also be employed as cooperative friendly jammers [25] that are able to send artificial noise (AN) (can be viewed as external interference) to assist the legitimate users

This work was supported in part by the National Key R&D Program of China under Grant 2020YFB1805005, in part by the National Natural Science Foundation of China under Grants 62001417, 91938202, 61831004 and 61971376, in part by the Zhejiang Provincial Natural Science Foundation of China under Grant LQ20F010010, in part by the Zhejiang Provincial Natural Science Foundation for Distinguished Young Scholars under Grant LR19F010002, in part by the State Key Laboratory of Rail Traffic Control and Safety (Contract No. RCS2020K010), Beijing Jiaotong University, and in part by the Fundamental Research Funds for the Central Universities under Grant 2019QNA5011. *(Corresponding authors: Ming-Min Zhao; Yunlong Cai.)*

K. Xu and M. M. Zhao are with the College of ISEE, Zhejiang University, Hangzhou 310027, China (e-mail: xukaidi13@126.com; zmmblack@zju.edu.cn). Y. Cai is with the College of ISEE, Zhejiang University, Hangzhou 310027, China, and also with the State Key Laboratory of Rail Traffic Control and Safety, Beijing Jiaotong University, Beijing 100044, China (e-mail: ylcai@zju.edu.cn). L. Hanzo is with the Department of ECS, University of Southampton, U.K. (Email: lh@ecs.soton.ac.uk).

L. Hanzo would like to acknowledge the financial support of the Engineering and Physical Sciences Research Council projects EP/N004558/1, EP/P034284/1, EP/P034284/1, EP/P003990/1 (COALESCE), of the Royal Society's Global Challenges Research Fund Grant as well as of the European Research Council's Advanced Fellow Grant QuantCom.

[2], [20]–[24]. Specifically, in [2], a dual-UAV-aided secure communication scheme has been proposed, where a second UAV was employed to jam a number of eavesdroppers on the ground. In [20], the impact of the UAV's jamming power and position on the outage probability and intercept probability have been examined. In order to improve the secrecy rate, in [21] a mobile UAV-aided jammer was harnessed for opportunistically interfering with the potential eavesdroppers. The authors of [22] studied the associated secrecy vs. energy efficiency maximization problem, where multiple source UAVs and jamming UAVs work cooperatively to serve the ground users. In [23], AN-beamforming and cooperative jamming were utilized, whilst only relying on location and statistical channel state information (CSI) of the eavesdroppers, where imperfect CSI knowledge of the link between the UAV-aided jammer and the destination was considered. Finally, the authors of [24] considered the worst-case secrecy rate maximization problem by taking into account the uncertainty of Eves location.

Against the above backdrop, we investigate a UAV-aided secure communication system, where the UAV transmits legitimate information to a ground-user Bob in the presence of a ground-based Eve. In contrast to prior studies, we conceive a power-splitting aided secure transmission scheme for protecting the UAV's communications. Explicitly, the UAV divides its transmit power into two parts, where a portion ρ of the signal power is used for transmitting confidential messages to Bob, while the remaining portion $1-\rho$ is devoted to transmitting AN to interfere with Eve's reception. Note that in the conventional secrecy communication systems operating without UAV-assiatnce, injecting AN has been widely applied for improving the secrecy transmission rates of Bob [26]–[28]. By relying on this power-splitting approach and exploiting the nimble mobility of the UAV, we aim for jointly optimizing the trajectory of the UAV and the communication/jamming power levels over time for maximizing the average secrecy rate of the UAV-Bob link, subject to the maximum UAV speed constraint, the total propulsion energy constraint, the total transmit power constraint, and other related constraints. To solve the resultant highly non-convex optimization problem efficiently, we propose a low-complexity iterative algorithm by combining the benefits of the block coordinate descent (BCD) method [29], the concave-convex procedure (CCCP) method [30] and the alternating direction method of multipliers (ADMM) [31].

Specifically, in order to address the related optimization variable coupling issues, we propose to decompose the original problem into two subproblems, i.e. the power allocation subproblem and the trajectory optimization subproblem, by applying the BCD method. The resultant subproblems, although much simplified compared to the original problem, they still remain non-convex. Therefore, by exploiting the fact that the underlying non-convex parts admit a difference-of-convex (DC) structure, we propose to transform them into more tractable forms with the aid of first-order approximations. We first show that a nearly closed-form optimal solution of the approximated power allocation subproblem can be devised by resorting to its Lagrangian dual problem. Then, by tactfully introducing auxiliary variables, the approximated trajectory optimization subproblem can be iteratively and globally solved by the ADMM method, and we demonstrate that each updating step therein can also be expressed in closed form. Given the fact that the existing algorithms suitable for solving joint power and trajectory optimization problems usually involve standard convex solvers, such as CVX [32], the proposed algorithm exhibits a very attractive and unique feature, namely that the optimization can be formulated almost in closed form, thus imposing a low computational complexity. Furthermore, the proposed algorithm is proved to be monotonically convergent. Our numerical results show the benefits of the power spitting approach proposed.

The main contributions of this treatise are as follows:

1) We formulate a joint power and trajectory optimization problem for a UAV-aided secure communication system relying on a power splitting approach for improving the secrecy performance.
2) To solve this challenging optimization problem, we propose a low-complexity iterative algorithm and show that each step in the proposed algorithm can be represented in a nearly closed form. Fyrthermore, we illustrate that the proposed algorithm can be easily extended to the case of 3D trajectory design.
3) We provide comprehensive numerical results for characterizing the efficiency of the proposed algorithm and the power splitting approach advocated. We then demonstrate the impact of the key system parameters on the average secrecy rate. In particular, we show that by appropriately splitting the transmit power of the UAV, the overall system performance can be substantially improved as compared to that without power splitting. Furthermore, compared to the existing algorithms using CVX, the running time of the proposed algorithm is at least 30 times lower.

This paper is structured as follows. In Section II, we introduce the considered UAV-enabled secure communication system and formulate the joint optimization problem. In Section III, we propose an efficient iterative algorithm to solve the considered problem with very low complexity and guaranteed convergence. Simulation results are presented in Section IV to show the effectiveness of our proposed algorithm and conclusions are drawn in Section V.

Notations: Scalars, vectors and matrices are respectively denoted by lower case, boldface lower case and boldface upper case letters. For a matrix $\mathbf{A}$, $\mathbf{A}^T$ denote its transpose. For a vector $\mathbf{a}$, $\|\mathbf{a}\|$ represents its Euclidean norm. $|\cdot|$ denotes the absolute value of any real or complex scalar. $\mathbb{R}^{m\times n}$ denotes the space of $m\times n$ real matrices. The set difference is defined as $\mathcal{A}\backslash\mathcal{B}\triangleq\{x|x\in\mathcal{A},x\notin\mathcal{B}\}$. $[x]^+\triangleq\max(x,0)$.

II. System model and Problem formulation

In this section, we introduce the system model and formulate the optimization problem of interest.

A. System Model

We consider a secure communication system where a UAV transmits confidential information to Bob in the presence of

a potential Eve, as shown in Fig. 1. In order to improve the security of the UAV-Bob link, the UAV also sends jamming signals (through injecting AN) to interfere Eves signal reception and increase the secrecy capacity.

Without loss of generality, we consider a 3D Cartesian coordinate system with Bob and Eve located at $(0,0,0)$ and $(L,0,0)$, respectively, i.e., Bob and Eve are both on the ground with a distance of L meters (m). For simplicity, we focus on the UAVs operation during a finite duration of N seconds (s) and ignore its take-off and landing phases. We further assume that the UAV is flying at a fixed altitude H, which is considered as the minimum altitude that is required for terrain or building avoidance.[1] Then, the time interval N is discretized into T equally spaced time slots, i.e., $N = T\delta_t$, where δ_t denotes the elemental slot length that is chosen to be sufficiently small. Thus, the time-varying trajectory of the UAV $(x(t), y(t), H)$ over the considered time period can be approximated by the T-length sequence $(x[i], y[i], H)$, $i \in \mathcal{T} \triangleq \{1, \cdots, T\}$, where $(x[i], y[i])$ denotes the UAVs $x-y$ coordinate at time slot i. Furthermore, let (x_1, y_1) and (x_T, y_T) denote the initial and final locations of the UAV and let $V_{\max}$ denote the maximum UAV speed, then we have the following mobility constraints:

$$x[1] = x_1,\ y[1] = y_1,\ x[T] = x_T,\ y[T] = y_T, \tag{1}$$

$$\frac{\sqrt{(x[i]-x[i+1])^2 + (y[i]-y[i+1])^2}}{\delta_t} \le V_{\max},\ \forall i \in \mathcal{T}\backslash T. \tag{2}$$

Besides, the UAV's mobility is also constrained by its energy budget. Specifically, the energy consumed by the UAV engine at time slot i is in proportion to the square of the velocity at this time slot and according to (2), the energy consumed by the UAV engine at time slot i, denoted as $E_{\text{mov}}[i]$, can be expressed as [33], [34]

$$E_{\text{mov}}[i] = \kappa((x[i]-x[i+1])^2 + (y[i]-y[i+1])^2), \tag{3}$$

where we have $\kappa = 0.5M\delta_t$ and M denotes the UAVs mass, including its payload. Thus, we have the following energy constraint for the mobility of the UAV:

$$\sum_{i=1}^{T-1} E_{\text{mov}}[i] \le E_{\text{tr}}, \tag{4}$$

where E_{tr} is the total mobility energy stored at the UAV, i.e., the UAVs energy budget.

We assume that the UAV altitude H is sufficiently large such that the LoS components dominate the channels of the UAV-Bob and UAV-Eve links, which is consistent with the channel models in the Third Generation Partnership Project (3GPP) TR 36.777 specification [35] (e.g., larger than 40 m in the rural macro with aerial vehicles (RMa-AV) scenario and 100 m in the urban macro with aerial vehicles (UMa-AV) scenario) and the channel measurement results in [36]. Therefore, we consider LoS channel models and the channel

[1]The proposed algorithm can also be extended to 3D trajectory optimization, which will become clear later.

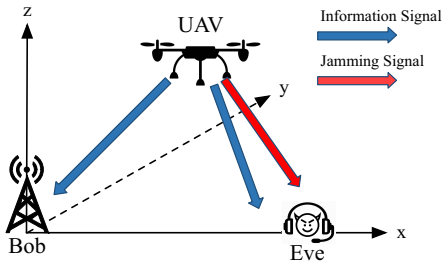

Fig. 1: The considered UAV-enabled secure communication system.

power gains of the UAV-Bob and UAV-Eve links at time slot i follow the free-space path loss model[2] given by [4], [14]

$$g_{\text{I}}[i] = \frac{\gamma_0}{d_{\text{I}}^2[i]},\ g_{\text{E}}[i] = \frac{\gamma_0}{d_{\text{E}}^2[i]}, \tag{5}$$

where γ_0 is the power gain at the reference distance of 1 m which depends on the carrier frequency and the antenna gains at the transmitter and receiver, $d_{\text{I}}[i]$ and $d_{\text{E}}[i]$ denote the distances from the UAV to Bob and Eve at time slot i, respectively, which can be expressed as

$$\begin{aligned} d_{\text{I}}[i] &= \sqrt{x^2[i] + y^2[i] + H^2}, \\ d_{\text{E}}[i] &= \sqrt{(x[i]-L)^2 + y^2[i] + H^2}. \end{aligned} \tag{6}$$

Let $p[i]$ denote the transmit power of the UAV at time slot i, we divide it into two parts where a portion of $p[i]\rho[i]$ is used for information transmission and the other $p[i](1-\rho[i])$ is utilized for transmitting AN to block Eve from successfully recovering the confidential information, where $\rho[i]$ is the power splitting ratio which satisfies

$$0 \le \rho[i] \le 1,\ \forall i \in \mathcal{T}. \tag{7}$$

Note that the AN can be eliminated by Bob but not necessarily by Eve [41]. The transmit power levels $\{p[i]\}$ are constrained by the limitation of both average power and peak power, which can be expressed as follows:

$$\frac{1}{T}\sum_{i=1}^{T} p[i] \le \bar{P}, \tag{8}$$

$$0 \le p[i] \le P_{\max},\ \forall i \in \mathcal{T}, \tag{9}$$

where $\bar{P}$ and $P_{\max}$ denote the average and peak power budgets, respectively. Equivalently, the average power constraint (8) can be rewritten as

$$\sum_{i=1}^{T} p[i] \le P, \tag{10}$$

where $P = T\bar{P}$ represents the total power available during the whole flight. Then, the signal-to-noise ratio (SNR) of the UAV-Bob link at time slot i is given by

$$\text{SNR}_{\text{I}}[i] \triangleq \frac{\gamma_0 p[i]\rho[i]}{d_{\text{I}}^2[i]\sigma^2}, \tag{11}$$

[2]There may exist other UAV-to-ground communication scenarios in practice, where the UAV-Bob/Eve channels follow the probabilistic LoS channel model [37]–[39] or the Rician channel model [40]. How to optimize the UAVs trajectory, the transmit power levels and the power splitting ratios with low complexity under these channel models and further investigation into the multi-antenna case are interesting topics that are left for future works.

where σ^2 is the additive white Gaussian noise (AWGN) variance at the receiver of Bob. Similarly, the signal-to-interference-plus-noise ratio (SINR) of the UAV-Eve link at time slot i can be expressed as

$$\begin{aligned}\mathrm{SINR_E}[i] &\triangleq \frac{\gamma_0 p[i]\rho[i]}{d_{\mathrm{E}}^2[i]\left(\frac{\gamma_0(1-\rho[i])p[i]}{d_{\mathrm{E}}^2[i]}+\sigma^2\right)} \\ &= \frac{\gamma_0 p[i]\rho[i]}{\gamma_0(1-\rho[i])p[i]+\sigma^2 d_{\mathrm{E}}^2[i]}.\end{aligned} \tag{12}$$

Based on (11) and (12), the secrecy rate of the UAV-Bob link at time slot i is given by [42]

$$R_{\mathrm{s}}[i] \triangleq [\log(1+\mathrm{SNR_I}[i]) - \log(1+\mathrm{SINR_E}[i])]^+, \tag{13}$$

and the average secrecy rate can be written as $R_{\mathrm{as}}(\{x[i],y[i],p[i],\rho[i]\}) \triangleq \frac{1}{T}\sum_{i=1}^{T} R_{\mathrm{s}}[i]$.

B. Problem Formulation

To this end, our objective is to maximize the average secrecy rate R_{as} subject to the UAVs mobility constraints in (1), (2) and (4), and the average and peak transmit power constraints in (10) and (9). Therefore, we can formulate the following optimization problem:

$$\begin{aligned}\max_{\{x[i],\,y[i],\,p[i],\,\rho[i]\}}\ & R_{\mathrm{as}}(\{x[i],y[i],p[i],\rho[i]\}) \\ \text{s.t. } & (1),\ (2),\ (4),\ (7),\ (9) \text{ and } (10),\end{aligned} \tag{14}$$

where the optimization variables include the UAV's trajectory $\{x[i],y[i]\}$, the transmit power levels $\{p[i]\}$ and the power splitting ratios $\{\rho[i]\}$.

Problem (14) is difficult to address due to the following two reasons. First, the operator $[\cdot]^+$ makes the objective function of problem (14) non-smooth. Second, the variables $\{p[i],\rho[i],x[i],y[i]\}$ are tightly coupled in the objective function, which makes problem (14) highly non-convex. Besides, even with fixed trajectory $\{x[i],y[i]\}$ and without $[\cdot]^+$, the variables $\{p[i]\}$ and $\{\rho[i]\}$ are still coupled in the objective function, therefore problem (14) is potentially more complex than the one considered in [14]. In the next section, instead of using the existing convex solvers such as CVX [32], we exploit the special structure of problem (14) and propose an efficient algorithm to tackle it with low complexity by blending the benefits of the BCD method, the CCCP method and the ADMM method.

III. Proposed Low-Complexity Algorithm

First, in order to handle the non-smoothness of the objective function of (14), we can simply ignore the operator $[\cdot]^+$ in the objective function since if the secrecy rate is negative at an arbitrary time slot, say l, we can always let the corresponding transmit power $p[l]$ be 0 such that $R_{\mathrm{s}}[l]=0$ is satisfied. Therefore, ignoring the operator $[\cdot]^+$ causes no loss of optimality for problem (14), and we can obtain the following equivalent problem:

$$\begin{aligned}\max_{\{x[i],\,y[i],\,p[i],\,\rho[i]\}}\ & \bar{R}_{\mathrm{as}}(\{x[i],y[i],p[i],\rho[i]\}) \\ \text{s.t. } & (1),\ (2),\ (4),\ (7),\ (9) \text{ and } (10),\end{aligned} \tag{15}$$

where

$$\begin{aligned}&\bar{R}_{\mathrm{as}}(\{x[i],y[i],p[i],\rho[i]\}) \\ &\triangleq \frac{1}{T}\sum_{i=1}^{T}\Big(\log\Big(1+\frac{\gamma_0 p[i]\rho[i]}{d_{\mathrm{I}}^2[i]\sigma^2}\Big) \\ &\quad -\log\Big(1+\frac{\gamma_0 p[i]\rho[i]}{\gamma_0(1-\rho[i])p[i]+\sigma^2 d_{\mathrm{E}}^2[i]}\Big)\Big).\end{aligned} \tag{16}$$

Then, it can be observed that the constraints of problem (15) are all convex, and the optimization variables are only coupled in the objective function. Thus, we can apply the BCD method to solve this problem by dividing the optimization variables into two blocks (i.e., $\{p[i],\rho[i]\}$ and $\{x[i],y[i]\}$) and optimizing them in an alternative manner. Specifically, with fixed trajectory, the power allocation subproblem can be expressed as

$$\begin{aligned}\max_{\{p[i],\,\rho[i]\}}\ & \bar{R}_{\mathrm{as}}(\{p[i]\},\{\rho[i]\}) \\ \text{s.t. } & (7),\ (9) \text{ and } (10),\end{aligned} \tag{17}$$

while by fixing the transmit power levels and power splitting ratios, the trajectory optimization subproblem can be written as

$$\begin{aligned}\max_{\{x[i],\,y[i]\}}\ & \bar{R}_{\mathrm{as}}(\{x[i],y[i]\}) \\ \text{s.t. } & (1),\ (2) \text{ and } (4).\end{aligned} \tag{18}$$

In other words, we can handle problem (15) by solving subproblems (17) and (18) iteratively, which yields a high-quality suboptimal solution, as detailed in the following two subsections.

A. Solving the Power Allocation Subproblem

In this subsection, we focus on problem (17) and propose to first convert it into a convex problem through proper transformation and approximation. Then, an efficient algorithm is presented to solve the resulting convex problem by employing the Lagrange duality method, where the basic idea is to build some complicated constraints into objective functions and then solve the dual problem instead of the original problem. It is worth mentioning that in [28], a similar power allocation/splitting optimization problem was considered (with a static transmitter and an additional energy harvesting constraint at the Eve), where both optimal and suboptimal solution were obtained and the approaches therein can also be employed to solve problem (17). However, the optimal solution in [28] requires a one-dimensional search to find the optimal power splitting ratio for each i while the suboptimal solution relies on an iterative procedure to alternately optimize the transmit power allocations and power splitting ratios, which both exhibit relatively high computational complexity. Note that compared with these existing methods, the proposed algorithm can provide lower computational complexity and by combining with the ellipsoid method, the proposed algorithm can also be easily extended to solve the problems in [28].

To proceed, we introduce two groups of auxiliary variables $a[i]$ and $b[i]$, which satisfy

$$a[i] = p[i]\rho[i],\ b[i] = p[i](1-\rho[i]). \tag{19}$$

As a result, problem (17) can be equivalently reformulated as

$$\max_{\{a[i],\, b[i]\}} \sum_{i=1}^{T} g_i(a[i], b[i]) \tag{20a}$$

$$\text{s.t. } a[i] + b[i] \le P_{\max},\ a[i] \ge 0,\ b[i] \ge 0,\ \forall i \in \mathcal{T}, \tag{20b}$$

$$\sum_{i=1}^{T} (a[i] + b[i]) \le P, \tag{20c}$$

where

$$\begin{aligned} g_i(a[i], b[i]) \triangleq & \log\left(1 + \frac{\gamma_0 a[i]}{d_{\mathrm{I}}^2[i]\sigma^2}\right) \\ & - \log\left(1 + \frac{\gamma_0 a[i]}{\gamma_0 b[i] + \sigma^2 d_{\mathrm{E}}^2[i]}\right). \end{aligned} \tag{21}$$

Although problem (20) is much simplified as compared with problem (17), it is still a non-convex problem which cannot be solved efficiently in general. However, it can be readily seen that $g_i(a[i], b[i])$ can be viewed as the subtraction of two concave terms, i.e., $\log\left(1 + \frac{\gamma_0 a[i]}{d_{\mathrm{I}}^2[i]\sigma^2}\right) + \log\left(\gamma_0 b[i] + \sigma^2 d_{\mathrm{E}}^2[i]\right)$ and $\log\left(\gamma_0 b[i] + \sigma^2 d_{\mathrm{E}}^2[i] + \gamma_0 a[i]\right)$, or equivalently, (20a) can be expressed in a DC form. Therefore, by employing the CCCP method [30], [43], [44], the lower bound of (20a) can be obtained as

$$\sum_{i=1}^{T} g_i(a[i], b[i]) \ge \sum_{i=1}^{T} \hat{g}_i(a[i], b[i]; a_f[i], b_f[i]), \tag{22}$$

where $\{a_f[i], b_f[i]\}$ is the given feasible solution of problem (17)[3] and

$$\begin{aligned} \hat{g}_i(a[i], b[i]; a_f[i], b_f[i]) \triangleq & \log\left(1 + \frac{\gamma_0 a[i]}{d_{\mathrm{I}}^2[i]\sigma^2}\right) \\ & - \log\left(\gamma_0 b_f[i] + \sigma^2 d_{\mathrm{E}}^2[i] + \gamma_0 a_f[i]\right) + \log\left(\gamma_0 b[i] + \sigma^2 d_{\mathrm{E}}^2[i]\right) \\ & - \frac{\gamma_0}{\gamma_0 b_f[i] + \sigma^2 d_{\mathrm{E}}^2[i] + \gamma_0 a_f[i]}(a[i] - a_f[i] + b[i] - b_f[i]). \end{aligned} \tag{23}$$

Note that the equality in (22) holds when $a[i] = a_f[i]$ and $b[i] = b_f[i]$. Consequently, problem (20) can be approximated by the following convex problem:

$$\begin{aligned} \max_{\{a[i],\, b[i]\}} & \sum_{i=1}^{T} \hat{g}_i(a[i], b[i]; a_f[i], b_f[i]) \\ & \text{s.t. (20b) and (20c).} \end{aligned} \tag{24}$$

Then, we note that without the total power constraint (20c), the other constraints in problem (24) are separable over different time slots $i \in \mathcal{T}$. Inspired by this observation, we introduce a Lagrange multiplier (dual variable) $\lambda \ge 0$ to (20c) and define the partial Lagrangian associated with problem (24) as [45]

$$\begin{aligned} \mathcal{L}(\{a[i]\}, \{b[i]\}, \lambda) = & \sum_{i=1}^{T} \hat{g}_i(a[i], b[i]; a_f[i], b_f[i]) \\ & - \lambda \sum_{i=1}^{T} (a[i] + b[i]) + \lambda P. \end{aligned} \tag{25}$$

[3]In the following, the subscript f is used to denote the feasible variable obtained in the previous BCD iteration.

With (25), the dual function, denoted by $d(\lambda)$, can be written as [45]

$$\begin{aligned} d(\lambda) \triangleq & \max_{\{a[i],\, b[i]\}} \mathcal{L}(\{a[i]\}, \{b[i]\}, \lambda) \\ & \text{s.t. (20b).} \end{aligned} \tag{26}$$

Let $\{a[i](\lambda)\}$ and $\{b[i](\lambda)\}$ denote an optimal solution of problem (26) with fixed λ. It is not difficult to see that, if $\{a[i](0), b[i](0)\}$ satisfy the total power constraint (20c), then $\{a[i](0), b[i](0)\}$ is optimal for problem (24), since when $\lambda = 0$, problem (26) becomes a relaxed version of problem (24) without the total power constraint (20c) and if (20c) is automatically satisfied in this case, the only possibility is that $\{a[i](0), b[i](0)\}$ is optimal. Otherwise, we need to increase λ to enhance the dominance of $-\lambda\sum_{i=1}^{T}(a[i] + b[i]) + \lambda P$ in $\mathcal{L}(\{a[i]\}, \{b[i]\}, \lambda)$ and force $\{a[i](\lambda), b[i](\lambda)\}$ to satisfy (20c).

Since problem (24) is convex and strong duality [45] holds, we have $p^{\text{opt}} = d(\lambda^{\text{opt}}) \le d(\lambda)$ for any $\lambda \ge 0$, where p^{opt} is the optimal objective value of problem (24) and λ^{opt} denotes the optimal dual variable. Hence, in order to solve problem (24), we can instead solve the following dual problem:

$$\min_{\lambda \ge 0}\ d(\lambda). \tag{27}$$

Since $d(\lambda)$ is a convex function with respect to λ and $P - \sum_{i=1}^{T}(a[i] + b[i])$ is a subgradient of $d(\lambda)$ [46, pp. 12], we can infer that if $\{a[i](\lambda^{\text{opt}}), b[i](\lambda^{\text{opt}})\}$ satisfies (20c) and $\lambda^{\text{opt}}\big(\sum_{i=1}^{T}(a[i](\lambda^{\text{opt}}) + b[i](\lambda^{\text{opt}})) - P\big) = 0$, then $\{a[i](\lambda^{\text{opt}}), b[i](\lambda^{\text{opt}})\}$ is an optimal solution of problem (24).

To this end, our main focus is on solving the dual problem (27) and this can be conducted by using the Bisection method [45] with the aid of the subgradient $P - \sum_{i=1}^{T}(a[i] + b[i])$. We summarize the proposed Lagrange duality method in Algorithm 1, where Steps 1-4 check whether or not $\{a[i](0), b[i](0)\}$ is the optimal solution, Steps 5-10 represent the Bisection method to solve the dual problem (27) globally. Note that in Step 9, we increase λ when the subgradient $P - \sum_{i=1}^{T}(a[i] + b[i])$ is positive and decrease λ otherwise, so as to find the optimal dual variable. In the following, we show that problem (26) can be solved globally in closed form with given λ.

Algorithm 1 Proposed Algorithm for Solving Problem (24)

1: Let $\lambda \leftarrow 0$ and solve problem (26) to obtain $\{a[i](0), b[i](0)\}$.
2: **if** $\sum_{i=1}^{T}(a[i](0) + b[i](0)) \le P$ **then**
3: **output** $\{a[i](0), b[i](0)\}$ and exit the algorithm.
4: **end if**
5: $\lambda_l \leftarrow 0$, find λ_r such that that $\sum_{i=1}^{T}(a[i](\lambda_r) + b[i](\lambda_r)) \le P$.
6: **repeat**
7: $\lambda \leftarrow (\lambda_l + \lambda_r)/2$.
8: Obtain $\{a[i](\lambda), b[i](\lambda)\}$ by solving problem (26).
9: **if** $\sum_{i=1}^{T}(a[i](\lambda) + b[i](\lambda)) < P$ **then** $\lambda_r \leftarrow \lambda$, **else** $\lambda_l \leftarrow \lambda$. **end if**
10: **until** $|\sum_{i=1}^{T}(a[i](\lambda) + b[i](\lambda)) - P|$ is less than a certain threshold.
11: **output** $(\{a[i](\lambda), b[i](\lambda)\}$.

It is readily seen that problem (26) can be divided into T independent subproblems for each time slot i. Since each subproblem can be solved similarly, we only need to focus on

one particular subproblem, and the corresponding optimization problem can be expressed as (the time slot index is omitted here for simplicity)

$$\begin{aligned} \max_{a,\ b}\ & \tilde{g}(a,b) \\ \text{s.t. } & a+b \le P_{\max},\ a \ge 0,\ b \ge 0, \end{aligned} \tag{28}$$

where $\tilde{g}(a,b) \triangleq \hat{g}(a,b;a_f,b_f) - \lambda(a+b)$. It can be observed that problem (28) is convex and there are only two optimization variables. With fixed a, $\tilde{g}(a,b)$ is a strictly concave function with respect to b since $\log(1+x)$ $(x \ge 0)$ is strictly concave. In what follows, we show how problem (28) can be efficiently solved with low complexity.

First, we recast problem (28) as the following equivalent two-tier maximization problem:

$$\max_{0\le a\le P_{\max}-b}\ \max_{0\le b\le P_{\max}-a}\ \tilde{g}(a,b). \tag{29}$$

For given a, the optimal b (it is unique since $\tilde{g}(a,b)$ is strictly concave with fixed a), denoted as $\bar{b}(a)$, can be obtained by resorting to the first-order optimality condition of the inner maximization problem, i.e.,

$$\frac{d\tilde{g}(a,b)}{db} = \frac{\gamma_0}{\gamma_0 b + \sigma^2 d_{\mathrm{E}}^2} - \frac{\gamma_0}{\gamma_0 b_f + \sigma^2 d_{\mathrm{E}}^2 + \gamma_0 a_f} - \lambda = 0, \tag{30}$$

and we can obtain the stationary point of $\tilde{g}(a,b)$ as $b_s = 1/C_b - \sigma^2 d_{\mathrm{E}}^2/\gamma_0$, where $C_b \triangleq \lambda + \frac{\gamma_0}{\gamma_0 b_f + \sigma^2 d_{\mathrm{E}}^2 + \gamma_0 a_f}$.

Since the inner maximization problem is a univariate convex problem with a bound constraint, its optimal objective value must be attained either on the boundary of the constraint or at the stationary point b_s. To be specific, the optimal solution of the inner maximization problem can be obtained by

$$\bar{b}(a) = \begin{cases} 0, \text{ if } b_s \le 0, \\ b_s, \text{ if } 0 < b_s < P_{\max} - a, \\ P_{\max} - a, \text{ otherwise.} \end{cases} \tag{31}$$

Substituting $\bar{b}(a)$ into the objective function of the outer maximization problem of (29), it can be recast as follows with a as the only variable:

$$\begin{aligned} \max_{a}\ & \bar{g}(a) \\ \text{s.t. } & a + \bar{b}(a) \le P_{\max},\ a \ge 0, \end{aligned} \tag{32}$$

where $\bar{g}(a) \triangleq \tilde{g}(a, \bar{b}(a))$. As discussed above, for a univariate optimization problem with a bound constraint, the optimal objective value must be attained at either the endpoints of the bound interval or some feasible stationary point of the objective function. Accordingly, the optimal value of problem (32) must be attained either at the point that satisfies $\frac{d\bar{g}(a)}{da} = 0$ $(0 < a < P_{\max} - \bar{b}(a))$, or $a \in \{0, P_{\max} - \bar{b}(a)\}$. Therefore, our basic idea to solve problem (32) is to search over all stationary points and boundary points and then choose the one that achieves the maximum objective value.

Next, we solve problem (32) by considering the above mentioned two cases. By taking the derivative of $\bar{g}(a)$ with respect to a, we have

$$\begin{aligned} \frac{d\bar{g}(a)}{da} =& \frac{\gamma_0}{\gamma_0 a + \sigma^2 d_{\mathrm{I}}^2} + \frac{\gamma_0 \frac{d\bar{b}(a)}{da}}{\gamma_0 \bar{b}(a) + \sigma^2 d_{\mathrm{E}}^2} \\ & - \Big(\frac{\gamma_0}{\gamma_0 b_f + \sigma^2 d_{\mathrm{E}}^2 + \gamma_0 a_f} + \lambda\Big)\Big(1 + \frac{d\bar{b}(a)}{da}\Big). \end{aligned} \tag{33}$$

*1) **Case I** ($0 < a < P_{max} - \bar{b}(a)$):* According to (31), we need to further consider the following two cases: $\bar{b}(a) = b_s$ or $\bar{b}(a) = 0$. For both cases, we have $\frac{d\bar{b}(a)}{da} = 0$. By plugging $\frac{d\bar{b}(a)}{da} = 0$ into (33) and letting (33) equal to 0, we have $\frac{\gamma_0}{\gamma_0 a + \sigma^2 d_{\mathrm{I}}^2} = \frac{\gamma_0}{\gamma_0 b_f + \sigma^2 d_{\mathrm{E}}^2 + \gamma_0 a_f} + \lambda$. Accordingly, a can be obtained by

$$a = \frac{\gamma_0 b_f + \sigma^2 d_{\mathrm{E}}^2 + \gamma_0 a_f}{\gamma_0 + \lambda(\gamma_0 b_f + \sigma^2 d_{\mathrm{E}}^2 + \gamma_0 a_f)} - \frac{d_{\mathrm{I}}^2 \sigma^2}{\gamma_0}. \tag{34}$$

*2) **Case II** ($a \in \{0, P_{max} - \bar{b}(a)\}$):* In this case, a can take on two possible values, i.e., $a = 0$ or $a = P_{\max} - \bar{b}(a)$. If $a = 0$, we have $b = \bar{b}(0)$, otherwise, if $a = P_{\max} - \bar{b}(a)$, this implies that $\bar{b}(a) = P_{\max} - a$ and $\frac{d\bar{b}(a)}{da} = -1$. Consequently, we have $\frac{d\bar{g}(a)}{da} = \frac{\gamma_0}{d_{\mathrm{I}}^2 \sigma^2 + \gamma_0 a} - \frac{\gamma_0}{d_{\mathrm{E}}^2 \sigma^2 + \gamma_0 (P_{\max} - a)} = 0$, which can be further simplified to a linear equation and its solution can be easily obtained by

$$a = \frac{(\sigma^2(d_{\mathrm{E}}^2 - d_{\mathrm{I}}^2) + \gamma_0 P_{\max})}{2\gamma_0}. \tag{35}$$

Then, by checking the abovementioned four sub-cases and discarding those do not satisfy the case conditions $0 < a < P_{\max} - \bar{b}(a)$ or $a \in \{0, P_{\max} - \bar{b}(a)\}$, we can obtain several feasible solutions of problem (28). Consequently, problem (28) can be globally solved in closed form by choosing the feasible solution that achieves the maximum objective value.

Together with Algorithm 1, the approximated power allocation subproblem (24) can be efficiently solved and with the optimized $\{a[i], b[i]\}$, we can easily obtain $\{p[i], \rho[i]\}$ according to (19).

B. Solving the Trajectory Optimization Subproblem

In this subsection, we focus on solving the trajectory optimization subproblem (18) with fixed $\{p[i], \rho[i]\}$. Note that although the constraints of problem (18) are convex, its objective function is non-concave with respect to $\{x[i], y[i]\}$ and it cannot be solved optimally in general. In order to resolve the difficulty caused by the non-concave objective function, we introduce two sets of auxiliary variables $\{u[i]\}$ and $\{t[i]\}$, which satisfy

$$u[i] \ge x^2[i] + y^2[i] + H^2,\ \forall i \in \mathcal{T}, \tag{36}$$

$$t[i] \le (x[i] - L)^2 + y^2[i] + H^2,\ \forall i \in \mathcal{T}. \tag{37}$$

As a result, we have the following equivalent optimization problem:

$$\begin{aligned} \max_{\{x[i],\ y[i],\ u[i],\ t[i]\}}\ & \tilde{R}_{\mathrm{as}}(u[i], t[i]) \\ \text{s.t. } & (1),\ (2),\ (4),\ (36) \text{ and } (37), \end{aligned} \tag{38}$$

where

$$\tilde{R}_{\text{as}}(u[i],t[i]) \triangleq \sum_{i=1}^{T}\Big(\log\Big(1+\frac{\gamma_0 p[i]\rho[i]}{u[i]\sigma^2}\Big) - \log\Big(1+\frac{\gamma_0 p[i]\rho[i]}{\gamma_0(1-\rho[i])p[i]+\sigma^2 t[i]}\Big)\Big). \tag{39}$$

We note that constraints (36) and (37) in problem (38) must be satisfied with equality at optimality since otherwise, we can always slightly decrease $u[i]$ and increase $t[i]$ such that a larger objective value can be achieved without violating any constraint. Therefore, problem (18) and problem (38) are equivalent.

It can be observed that the term $\log\Big(1+\frac{\gamma_0 p[i]\rho[i]}{u[i]\sigma^2}\Big)$ in $\tilde{R}_{\text{as}}(u[i],t[i])$ and the term $(x[i]-L)^2+y^2[i]$ in (37) are convex with respect to $u[i]$ and $\{x[i],y[i]\}$, respectively. Therefore, although $\tilde{R}_{\text{as}}(u[i],t[i])$ is non-concave and constraint (37) is non-convex, they can be expressed in DC forms and problem (38) can be addressed by employing the CCCP method. Specifically, we propose to approximate problem (38) to a convex one and then present an ADMM-based algorithm to solve it globally. First, the proposed algorithm assumes a given solution $\{x_f[i],y_f[i],u_f[i],t_f[i]\}$ in the previous BCD iteration which is feasible to (38). Then, by employing the first-order Taylor approximation, we construct the lower bounds for $(x[i]-L)^2+y^2[i]+H^2$ and $\log\Big(1+\frac{\gamma_0 p[i]\rho[i]}{u[i]\sigma^2}\Big)$ as follows:

$$\begin{aligned}-x_f^2[i]+2x_f[i]x[i]-2x[i]L+L^2-y_f^2[i]\\ +2y_f[i]y[i]+H^2 \le (x[i]-L)^2+y^2[i]+H^2,\end{aligned} \tag{40}$$

$$\begin{aligned}\log\Big(1+\frac{\gamma_0 p[i]\rho[i]}{u[i]\sigma^2}\Big) \ge \log(1+\frac{\gamma_0 p[i]\rho[i]}{u_f[i]\sigma^2})\\ -\frac{\gamma_0 p[i]\rho[i](u[i]-u_f[i])}{u_f^2[i]\sigma^2+\gamma_0 p[i]\rho[i]u_f[i]}.\end{aligned} \tag{41}$$

Similarly, we also approximate the second term in (39), i.e., $\varpi(t[i]) \triangleq \log\Big(1+\frac{\gamma_0 p[i]\rho[i]}{\gamma_0(1-\rho[i])p[i]+\sigma^2 t[i]}\Big)$, and obtain the following upper bound:

$$\begin{aligned}&\log\Big(1+\frac{\gamma_0 p[i]\rho[i]}{\gamma_0(1-\rho[i])p[i]+\sigma^2 t[i]}\Big)\\ &=\log(\gamma_0 p[i]+\sigma^2 t[i]) - \log\big(\gamma_0(1-\rho[i])p[i]+\sigma^2 t[i]\big)\\ &\le \log(\gamma_0 p[i]+\sigma^2 t_f[i]) + \frac{\sigma^2(t[i]-t_f[i])}{t_f[i]\sigma^2+\gamma_0 p[i]}\\ &\quad -\log(\gamma_0 p[i](1-\rho[i])+\sigma^2 t[i]).\end{aligned} \tag{42}$$

Note that although replacing $\varpi(t[i])$ by its upper bound in (42) is mathematically unnecessary since it is already a convex function, it will be clear later that with this approximation, the resulting problem is easier to handle. Moreover, we will show in the simulation results that even with such additional approximation, the performance achieved by the proposed low-complexity algorithm is similar to that achieved by using the CVX solver. After the above mentioned approximations, it is not difficult to see that the original non-concave objective function $\tilde{R}_{\text{as}}(u[i],t[i])$ and non-convex constraint (37) in problem (38) can be approximated by

$$\begin{aligned}t[i] \le -x_f^2[i]+2x_f[i]x[i]-2x[i]L+L^2\\ -y_f^2[i]+2y_f[i]y[i]+H^2,\ \forall i\in\mathcal{T},\end{aligned} \tag{43}$$

$$\begin{aligned}&\check{R}_{\text{as}}(u[i],t[i])\\ &\triangleq \sum_{i=1}^{T}\Big(-\frac{\gamma_0 p[i]\rho[i](u[i]-u_f[i])}{u_f^2[i]\sigma^2+\gamma_0 p[i]\rho[i]u_f[i]}\\ &\quad -\frac{\sigma^2(t[i]-t_f[i])}{t_f[i]\sigma^2+\gamma_0 p[i]}+\log(\gamma_0 p[i](1-\rho[i])+\sigma^2 t[i])\Big),\end{aligned} \tag{44}$$

respectively.[4] Therefore, problem (38) can be approximated as the following convex problem:

$$\begin{aligned}\max_{\{x[i],\,y[i],\,u[i],\,t[i]\}}\ &\check{R}_{\text{as}}(u[i],t[i])\\ \text{s.t. }&(1),\ (2),\ (4),\ (36)\text{ and }(43).\end{aligned} \tag{45}$$

It is noteworthy that the approximation in (42) will not affect the convergence of the proposed algorithm [47], since the resultant objective function $\check{R}_{\text{as}}(u[i],t[i])$ is a global lower bound of $\tilde{R}_{\text{as}}(u[i],t[i])$ and the first-order behaviors of $\check{R}_{\text{as}}(u[i],t[i])$ and $\tilde{R}_{\text{as}}(u[i],t[i])$ are the same at the point of approximation.

Subsequently, we develop a low-complexity ADMM-based algorithm to globally solve problem (45) efficiently. By exploiting the special structure of problem (45), we show that by tactfully introducing auxiliary variables, it can be efficiently solved and each step in the proposed ADMM method can be carried out in closed form. For completeness, a brief introduction of the ADMM method is provided in Appendix A. It can be seen that problem (45) is not in the standard form of problem (66), therefore, it is difficult to directly apply the ADMM method. The main difficulties lie in: 1) how to partition the optimization variables of problem (45) into two groups, as in the ADMM framework, 2) how to decompose each group problem for much easier implementation. To proceed, we introduce four redundancy copies of the variables $\{x[i],y[i]\}$ to help address the abovementioned difficulties, i.e.,

$$x[i]=\bar{x}[i],\ y[i]=\bar{y}[i],\ x[i]=\tilde{x}[i],\ y[i]=\tilde{y}[i], \tag{46a}$$

$$x[i]=\hat{x}[i],\ y[i]=\hat{y}[i],\ \hat{x}[i]=\ddot{x}[i],\ \hat{y}[i]=\ddot{y}[i],\ \forall i\in\mathcal{T}. \tag{46b}$$

Then, due to the introduction of (46), constraints (2), (4), (36) and (43) are modified as follows without loss of optimality:

$$(x[i]-\bar{x}[i+1])^2+(y[i]-\bar{y}[i+1])^2 \le V_{\max}^2\delta_t^2,\ \forall i\in\mathcal{T}\backslash T, \tag{47}$$

$$\sum_{n=1}^{T-1}\big((\ddot{x}[i]-\ddot{x}[i+1])^2+(\ddot{y}[i]-\ddot{y}[i+1])^2\big) \le \frac{E_{\text{tr}}}{\kappa}, \tag{48}$$

$$u[i] \ge \tilde{x}^2[i]+\tilde{y}^2[i]+H^2,\ \forall i\in\mathcal{T}, \tag{49}$$

$$\begin{aligned}t[i] \le -\tilde{x}_f^2[i]+2\tilde{x}_f[i]x[i]-2\tilde{x}[i]L+L^2\\ -\tilde{y}_f^2[i]+2\tilde{y}_f[i]\tilde{y}[i]+H^2,\ \forall i\in\mathcal{T}.\end{aligned} \tag{50}$$

[4]Note that in (44), some constant terms are ignored for simplicity.

Next, by dualizing and penalizing the equality constraints in (46) to the objective function, we can obtain the augmented Lagrangian (AL) function of problem (45), which is given by

$$\begin{aligned} L_\delta(\mathcal{Q},\mathcal{U}) = \check{R}_{\text{as}}(u[i],t[i]) - \frac{\delta}{2}\sum_{i=1}^{T}\Big((x[i]-\bar{x}[i]-\lambda_{x_i}/\delta)^2 \\ + (y[i]-\bar{y}[i]-\lambda_{y_i}/\delta)^2 + (x[i]-\tilde{x}[i]-\eta_{x_i}/\delta)^2 \\ + (y[i]-\tilde{y}[i]-\eta_{y_i}/\delta)^2 + (x[i]-\hat{x}[i]-\omega_{x_i}/\delta)^2 \\ + (y[i]-\hat{y}[i]-\eta_{y_i}/\delta)^2 + (\hat{x}[i]-\ddot{x}[i]-\theta_{x_i}/\delta)^2 \\ + (\hat{y}[i]-\ddot{y}[i]-\theta_{y_i}/\delta)^2\Big), \end{aligned} \tag{51}$$

where $\mathcal{Q} \triangleq \{x[i], y[i], \bar{x}[i], \bar{y}[i], \hat{x}[i], \hat{y}[i], \tilde{x}[i], \tilde{y}[i], \ddot{x}[i], \ddot{y}[i], u[i], t[i]\}$, δ is the penalty parameter, $\mathcal{U} \triangleq \{\lambda_{x_i}, \lambda_{y_i}, \eta_{x_i}, \eta_{y_i}, \omega_{x_i}, \omega_{y_i}, \theta_{x_i}, \theta_{y_i}\}$, $\{\lambda_{x_i}, \lambda_{y_i}\}$, $\{\eta_{x_i}, \eta_{y_i}\}$, $\{\omega_{x_i}, \omega_{y_i}\}$ and $\{\theta_{x_i}, \theta_{y_i}\}$ are the dual variables associated with the constraints in (46), respectively. Accordingly, we have the following AL problem:

$$\begin{aligned} \max_{\mathcal{Q}}\ & L_\delta(\mathcal{Q},\mathcal{U}) \\ \text{s.t. }& (1),\ (46)-(50). \end{aligned} \tag{52}$$

Note that in (51), we have dualized and penalized the equality constraints in (46), and moreover added some constant terms in order to complete the square terms. The added constants will not affect the optimality of the AL problem (52).

To solve problem (52), we need to divide the primal variables $\mathcal{Q}$ into two groups (corresponding to $\mathbf{x}$ and $\mathbf{z}$ in Appendix A), as the ADMM can diverge for certain pathological problems when the number of blocks is larger than two [48]. For this purpose and to facilitate parallel implementation, we group the variables $\mathcal{Q}\backslash\{\ddot{x}[i], \ddot{y}[i]\}$ according to the parity of their corresponding time slot indices, while the variables $\{\ddot{x}[i], \ddot{y}[i]\}$ are handled in one group since they all appear in constraint (48). Besides, we also classify these variables into three different types according to the forms of their corresponding optimization subproblems, as shown in Fig. 2. In the following, we elaborate the details on how to solve these subproblems efficiently.

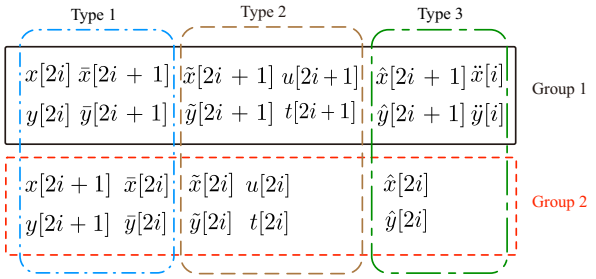

Fig. 2: Grouping and classification of the optimization variables.

1) Group 1: The Type 1 subproblem is involved with variables $\{x[2i], \bar{x}[2i+1], y[2i], \bar{y}[2i+1]\}$ and the corresponding optimization problem can be expressed as

$$\begin{aligned} \max_{x[2i],\ \bar{x}[2i+1],\ y[2i],\ \bar{y}[2i+1]}\ & L_{\delta,1} \\ \text{s.t. }& (x[2i]-\bar{x}[2i+1])^2 + (y[2i]-\bar{y}[2i+1])^2 \le V_{\max}^2\delta_t^2, \end{aligned} \tag{53}$$

where $L_{\delta,1} \triangleq -\frac{\delta}{2}\Big((x[2i]-\bar{x}[2i]-\frac{\lambda_{x_{2i}}}{\delta})^2 + (y[2i]-\bar{y}[2i]-\frac{\lambda_{y_{2i}}}{\delta})^2 + (x[2i]-\tilde{x}[2i]-\frac{\eta_{x_{2i}}}{\delta})^2 + (y[2i]-\tilde{y}[2i]-\frac{\eta_{y_{2i}}}{\delta})^2 + (x[2i]-\hat{x}[2i]-\frac{\omega_{x_{2i}}}{\delta})^2 + (y[2i]-\hat{y}[2i]-\frac{\omega_{y_{2i}}}{\delta})^2 + (x[2i+1]-\bar{x}[2i+1]-\frac{\lambda_{x_{2i+1}}}{\delta})^2 + (y[2i+1]-\bar{y}[2i+1]-\frac{\lambda_{y_{2i+1}}}{\delta})^2\Big)$. Problem (53) is a quadratically constrained quadratic programming (QCQP) problem with only one constraint, therefore, it can be globally solved and the detailed derivation of its optimal solution is relegated to Appendix B. Note that for each time slot i, the corresponding variables can be optimized in parallel.

The Type 2 subproblem involves the optimization of $\{\tilde{x}[2i+1], \tilde{y}[2i+1], u[2i+1], t[2i+1]\}$, which can be written as

$$\begin{aligned} \max_{\tilde{x}[2i+1],\ \tilde{y}[2i+1],\ u[2i+1],\ t[2i+1]}\ & L_{\delta,2} \\ \text{s.t. } & u[2i+1] \ge \tilde{x}^2[2i+1] + \tilde{y}^2[2i+1] + H^2, \\ & t[2i+1] \le -\tilde{x}_f^2[2i+1] + 2\tilde{x}_f[2i+1]\tilde{x}[2i+1] \\ & \qquad + L^2 - 2\tilde{x}[2i+1]L - \tilde{y}_f^2[2i+1] \\ & \qquad + 2\tilde{y}_f[2i+1]\tilde{y}[2i+1] + H^2, \end{aligned} \tag{54}$$

where $L_{\delta,2} \triangleq -a[2i+1]u[2i+1] - \frac{\sigma^2 t[2i+1]}{t_f[2i+1]+\gamma_0 p[2i+1]} + \log(\gamma_0(1-\rho[2i+1])p[2i+1] + \sigma^2 t[2i+1]) - \frac{\delta}{2}\big((x[2i+1]-\tilde{x}[2i+1]-\frac{\omega_{x_{2i+1}}}{\delta})^2 + (y[2i+1]-\tilde{y}[2i+1]-\frac{\omega_{y_{2i+1}}}{\delta})^2\big)$ and $a[2i+1] = \frac{\gamma_0 p[2i+1]\rho[2i+1]}{u_f^2[2i+1]\sigma^2+\gamma_0 p[2i+1]\rho[2i+1]u_f[2i+1]}$. It can be observed that problem (54) is a convex problem with two quadratic constraints. Although there is no closed-form solution for such kind of optimization problems in general, we show that it can be efficiently solved in closed form by exploiting its special structure and the details are provided in Appendix C. It is important to note that this closed-form solution is easier to obtain when the term $\varpi(t[i])$ in (39) is approximated by its upper bound in (42); otherwise, the derivation would be very involved as the gradient of $\varpi(t[i])$ with respect to $t[i]$ is $\frac{1}{\gamma_0 p[i]+\sigma^2 t[i]} - \frac{1}{\gamma_0(1-\rho[i])p[i]+\sigma^2 t[i]}$ and the Lagrangian function associated with problem (76) would be a quadratic function of $t[i]$, thus rendering it difficult to obtain the optimal dual variable.

The Type 3 subproblem involves the optimization of $\{\hat{x}[2i+1], \hat{y}[2i+1], \ddot{x}[i], \ddot{y}[i]\}$ and we can obtain the following problem:

$$\begin{aligned} \max_{\{\hat{x}[2i+1],\ \hat{y}[2i+1],\ \ddot{x}[i],\ \ddot{y}[i]\}}\ & L_{\delta,3} \\ \text{s.t. } (1),\ & \sum_{n=1}^{T-1}\left((\ddot{x}[i]-\ddot{x}[i+1])^2 + (\ddot{y}[i]-\ddot{y}[i+1])^2\right) \le \frac{E_{\text{tr}}}{\kappa}, \end{aligned} \tag{55}$$

where $L_{\delta,3} \triangleq -\frac{\delta}{2}\sum_{n=1}^{T}\Big((\hat{x}[i]-\ddot{x}[i]-\frac{\theta_{x_i}}{\delta})^2 + (\hat{y}[i]-\ddot{y}[i]-\frac{\theta_{y_i}}{\delta})^2 + (x[i]-\hat{x}[i]-\frac{\eta_{x_i}}{\delta})^2 + (y[i]-\hat{y}[i]-\frac{\eta_{y_i}}{\delta})^2\Big)$. Similar to problem (53), problem (55) is also a convex QCQP problem with only one constraint and strong duality holds for this problem. Therefore, it can be globally solved in closed form and the details are presented in Appendix D.

2) Group 2: The Type 1 subproblem in group 2 can be obtained by changing the time slot indices in problem (53) from $2i$ and $2i+1$ to $2i+1$ and $2i+2$, respectively. Therefore, it can be solved by resorting to Appendix B, the details are not shown here for brevity. Similarly, the Type 2 subproblem can be obtained by changing the time slot indices in problem

(54) and it can be efficiently solved according to Appendix C. Besides, the Type 3 subproblem is given by

$$\max_{\{\hat{x}[2i],\, \hat{y}[2i]\}} L_{\delta,3}. \tag{56}$$

Since problem (56) is an unconstrained convex problem, its global optimal solution can be easily obtained by (resorting to the first-order optimality condition)

$$\begin{aligned} \hat{x}^{\text{opt}}[2i] &= \frac{\ddot{x}[2i] + x[2i]}{2} + \frac{\theta_{x_{2i}} - \eta_{x_{2i}}}{2\delta}, \\ \hat{y}^{\text{opt}}[2i] &= \frac{\ddot{y}[2i] + y[2i]}{2} + \frac{\theta_{y_{2i}} - \eta_{y_{2i}}}{2\delta}. \end{aligned} \tag{57}$$

Finally, the dual variables can be updated by

$$\begin{aligned} &\lambda_{x_i} = \lambda_{x_i} + \delta(\bar{x}[i] - x[i]),\ \lambda_{y_i} = \lambda_{y_i} + \delta(\bar{y}[i] - y[i]), \\ &\eta_{x_i} = \eta_{x_i} + \delta(\hat{x}[i] - x[i]),\ \eta_{y_i} = \eta_{y_i} + \delta(\hat{y}[i] - y[i]), \\ &\omega_{x_i} = \omega_{x_i} + \delta(\tilde{x}[i] - x[i]),\ \omega_{y_i} = \omega_{y_i} + \delta(\tilde{y}[i] - y[i]), \\ &\theta_{x_i} = \theta_{x_i} + \delta(\ddot{x}[i] - \hat{x}[i]),\ \theta_{y_i} = \theta_{y_i} + \delta(\ddot{y}[i] - \hat{y}[i]). \end{aligned} \tag{58}$$

Overall, the proposed algorithm to solve problem (45) is summarized in Algorithm 2. Note that if the 3D trajectory optimization is considered, we can similarly introduce auxiliary variables for the altitudes of the UAV and solve the resulting subproblems accordingly without much difficulty.

Algorithm 2 Proposed ADMM Method for Problem (45)

1: Let $\mathcal{U} = \mathbf{0}$, set a threshold ϵ and the penalty parameter δ.
2: **repeat**
3: Update the variables in group 1 by solving subproblems (53), (54) and (55).
4: Change the time slot indices in subproblems (53) and (54) and update the variables in group 2 by solving subproblems (53), (54) and (56).
5: Update the dual variables according to (58)
6: Calculate the primal residual $\mathbf{r}$ and dual residual $\mathbf{s}$ using (69).
7: **until** $\max(\|\mathbf{r}\|, \|\mathbf{s}\|) < \epsilon$.
8: **output** $\{x[i], y[i]\}$.

C. Overall Algorithm and Analysis

To summarize, the proposed algorithm can find a suboptimal solution of problem (15) by applying the BCD method, i.e., the power allocation subproblem (17) and the trajectory optimization subproblem (18) are solved alternately in an iterative manner. The detailed steps of the proposed algorithm are listed in Algorithm 3. Furthermore, regarding to the convergence of Algorithm 3, we have the following proposition:

Proposition 1. The sequence of the objective values generated by Algorithm 3 is guaranteed to converge.

Proof. Since problems (17) and (18) are equivalent to problems (20) and (38), respectively, and the latter two can be approximated by problems (24) and (45) through the first-order approximations, we can infer that the solution obtained in the $(t-1)$-th iteration of Algorithm 3, denoted by $\{p^{t-1}[i], \rho^{t-1}[i], x^{t-1}[i], y^{t-1}[i]\}$, is feasible to problem (15). Besides, due to the fact that Algorithm 1 and Algorithm 2 can obtain the optimal solutions of problems (24) and (45), respectively, it can be readily seen that $\bar{R}_{\text{as}}(\{x^t[i], y^t[i], p^t[i], \rho^t[i]\}) \geq \bar{R}_{\text{as}}(\{x^{t-1}[i], y^{t-1}[i], p^{t-1}[i], \rho^{t-1}[i]\})$. Together with the fact that the objective value of problem (15) is upper bounded by a certain value due to the power constraints (8) and (9), we conclude that the sequence $\{\bar{R}_{\text{as}}(\{x^t[i], y^t[i], p^t[i], \rho^t[i]\})\}$ guarantees to converge. This completes the proof. □

Algorithm 3 Proposed Algorithm for Problem (15)

1: Initialize $\mathcal{Q}$, $\{p[i], \rho[i]\}$ and set a threshold τ.
2: **repeat**
3: Solve problem (24) using Algorithm 1 with fixed trajectory and obtain $\{p[i], \rho[i]\}$.
4: Solve problem (45) using Algorithm 2 with fixed $\{p[i], \rho[i]\}$ and obtain $\mathcal{Q}$.
5: $\mathcal{Q}_f \leftarrow \mathcal{Q}$, $\{p_f[i], \rho_f[i]\} \leftarrow \{p[i], \rho[i]\}$.
6: **until** The fractional increase of the objective value of problem (15) is below the threshold τ.
7: **output** $\{p[i], \rho[i], x[i], y[i]\}$.

Besides, Algorithm 3 exhibits very low computational complexity and the detailed analysis is presented as follows. As mentioned in Section III-A, since the power allocation subproblem is divided into T independent subproblems and each subproblem is solved efficiently in closed form, the worst-case complexity of Algorithm 1 is $\mathcal{O}(N_B T)$, where N_B denotes the number of iterations required by the Bisection method. For Algorithm 2, we can see that its complexity is dominated by solving problem (55) using Gaussian eliminations. Since the complexity of solving one instance of problem (55) scales with T, the complexity of Algorithm 2 can be expressed as $\mathcal{O}(N_A N_B T)$, where N_A denotes the number of ADMM iterations. In summary, the complexity of Algorithm 3 can be expressed as $\mathcal{O}(N_{\text{BCD}}(N_A N_B T + N_B T))$, where N_{BCD} represents the number of BCD iterations. Note that the complexity of the conventional algorithm in [14] is $\mathcal{O}(N_{\text{BCD}} T^{3.5})$, therefore, the proposed Algorithm 3 exhibits a much lower complexity[5] and it will be shown in Section IV that Algorithm 3 can achieve a similar performance with that of the conventional algorithm using existing convex solvers.

D. Extension to 3D Trajectory Design

In this subsection, we extend the proposed algorithm to the case of 3D trajectory design, where the UAV's time-varying altitudes are also treated as optimization variables. In this case, problem (15) becomes:

$$\begin{aligned} \max_{\{x[i],\, y[i],\, z[i],\, p[i],\, \rho[i]\}} \ & \bar{R}_{\text{as}}^{\text{3D}}(\{x[i], y[i], z[i], p[i], \rho[i]\}) \\ \text{s.t. } & (1),\ (4),\ (7),\ (9) \text{ and } (10), \\ & z[1] = z_1,\ z[T] = z_T,\ z_{\min} \leq z[i] \leq z_{\max},\ \forall i \in \mathcal{T}, \\ & ((x[i] - x[i+1])^2 + (y[i] - y[i+1])^2 \\ & \quad + (z[i] - z[i+1])^2)^{\frac{1}{2}} / \delta_t \leq V_{\max},\ \forall i \in \mathcal{T} \backslash T, \end{aligned} \tag{59}$$

where $\bar{R}_{\text{as}}^{\text{3D}}(\{x[i], y[i], z[i], p[i], \rho[i]\}) \triangleq \frac{1}{T} \sum_{i=1}^{T} \left(\log\left(1 + \frac{\gamma_0 p[i] \rho[i]}{d_{\text{I3}}^2[i] \sigma^2}\right) - \log\left(1 + \frac{\gamma_0 p[i] \rho[i]}{\gamma_0 (1 - \rho[i]) p[i] + \sigma^2 d_{\text{E3}}^2[i]}\right)\right)$, $d_{\text{I3}}^2[i] \triangleq x[i]^2 +$

[5]Since T is usually on the order of several hundreds, thus $T^{3.5} \gg N_A N_B T$.

$y[i]^2+z[i]^2$, $d_{\text{E3}}^2[i] \triangleq (x[i]-L)^2+y[i]^2+z[i]^2$, $z_{\min}$ and $z_{\max}$ denote the UAVs minimally and maximally allowed altitudes, respectively, while z_1 and z_T are the initial and final altitudes of the UAV, respectively. Let $\bar{R}_{\text{as}}^{\text{3D}}(\{x[i], y[i], z_{\min}, p[i], \rho[i]\})$ denote the average secrecy rate with the altitudes of the UAV fixed to $z[i] = z_{\min}, \forall i \in \mathcal{T}$, then we have the following proposition:

Proposition 2. For all possible trajectories $\{x[i], y[i], z[i]\}$ of problem (59), we have

$$\begin{aligned}\bar{R}_{\text{as}}^{\text{3D}}(\{x[i], y[i], z_{\min}, p[i], \rho[i]\}) \\ \geq \bar{R}_{\text{as}}^{\text{3D}}(\{x[i], y[i], z[i], p[i], \rho[i]\}).\end{aligned} \tag{60}$$

Proof. Please refer to Appendix E. □

Proposition 2 implies that the UAV will try to fly as low as possible to obtain a better performance according to (60), thus we can safely ignore the constraints $z[i] \leq z_{\max}, \forall i \in \mathcal{T}$ without loss of optimality.

We first consider the special case when the initial and final altitudes of the UAV are set to $z_{\min}$, i.e., $z[1] = z[T] = z_{\min}$. According to Proposition 2, we can directly set the altitude of the UAV at each time slot to $z_{\min}$, then it can be readily seen that problem (59) reduces to problem (15) in this case and can be efficiently solved by Algorithm 3.

For the general case when the initial and final altitudes of the UAV are not necessarily at $z_{\min}$, we have an addition sequence of optimization variables, i.e., $\{z[i]\}$, in problem (59) as compared to those in problem (15). Since the power allocation subproblem is similar to the 2D case, we mainly focus on the trajectory optimization subproblem in the sequel. In particular, similar to the idea in (46), we further introduce auxiliary variables $\{\bar{z}[i], \tilde{z}[i], \hat{z}[i], \ddot{z}[i]\}$ which satisfy $\bar{z}[i] = \tilde{z}[i] = \hat{z}[i] = \ddot{z}[i] = z[i], \forall i \in \mathcal{T}$. Accordingly, constraints (47)-(50) are modified as follows:

$$\begin{aligned}(x[i]-\bar{x}[i+1])^2+(y[i]-\bar{y}[i+1])^2 \\ +(z[i]-\bar{z}[i+1])^2 \leq V_{\max}^2\delta_t^2,\ \forall i \in \mathcal{T}\backslash T,\end{aligned} \tag{61}$$

$$\begin{aligned}\sum_{n=1}^{T-1}\big((\ddot{x}[i]-\ddot{x}[i+1])^2+(\ddot{y}[i]-\ddot{y}[i+1])^2 \\ +(\ddot{z}[i]-\ddot{z}[i+1])^2\big) \leq \frac{E_{\text{tr}}}{\kappa},\end{aligned} \tag{62}$$

$$u[i] \geq \tilde{x}^2[i]+\tilde{y}^2[i]+\tilde{z}^2[i],\ \forall i \in \mathcal{T}, \tag{63}$$

$$\begin{aligned}t[i] \leq -\tilde{x}_f^2[i]+2\tilde{x}_f[i]x[i]-2\tilde{x}[i]L+L^2-\tilde{y}_f^2[i] \\ +2\tilde{y}_f[i]\tilde{y}[i]-\tilde{z}_f^2[i]+2\tilde{z}_f[i]\tilde{z}[i],\ \forall i \in \mathcal{T}.\end{aligned} \tag{64}$$

We note that the grouping/classification of the variables and the optimization of these variables can be similarly conducted as those in the 2D case with proper modifications. Take the 3D version of problem (54) as an example, by following the derivation in Appendix C, problem (76) becomes

$$\begin{aligned}\max_{\tilde{x},\,\tilde{y},\,\tilde{z},\,t}\ & L_{\delta,2,z} \\ \text{s.t. } & t \leq -\tilde{x}_f^2+2\tilde{x}_f\tilde{x}+L^2-2\tilde{x}L-\tilde{y}_f^2 \\ & \quad +2\tilde{y}_f\tilde{y}-\tilde{z}_f^2+2\tilde{z}_f\tilde{z}, \\ & \tilde{z} \geq z_{\min},\end{aligned} \tag{65}$$

where $L_{\delta,2,z} \triangleq -a(\tilde{x}^2+\tilde{y}^2+\tilde{z}^2)-\frac{\sigma^2 t}{t_f+\gamma_0 p}+\log(\gamma_0(1-\rho)p+\sigma^2 t)-\frac{\delta}{2}\big((x-\tilde{x}-\frac{\omega_x}{\delta})^2+(y-\tilde{y}-\frac{\omega_y}{\delta})^2+(z-\tilde{z}-\frac{\omega_z}{\delta})^2\big)$ and ω_z is similarly defined as ω_x and ω_y. The corresponding Lagrange function can be expressed as $L_{\delta,2,z,\tilde{\mu}} \triangleq L_{\delta,2,z}+\tilde{\mu}\big(-\tilde{x}_f^2+2\tilde{x}_f\tilde{x}+L^2-2\tilde{x}L-\tilde{y}_f^2+2\tilde{y}_f\tilde{y}-\tilde{z}_f^2+2\tilde{z}_f\tilde{z}-t\big)$, where $\tilde{\mu}$ is the Lagrangian dual variable. By checking the first-order optimality condition of problem (65), we can see that the optimal solutions of $\tilde{x}, \tilde{y}$ and t are the same as (77), while the optimal $\tilde{z}$ can be expressed as $\tilde{z}^{\text{opt}}(\tilde{\mu}) = \max\left(\frac{\delta z-\omega_z+2\tilde{\mu}\tilde{z}_f}{2a+\delta}, z_{\min}\right)$. If the solution $\{\tilde{x}^{\text{opt}}(0), \tilde{y}^{\text{opt}}(0), \tilde{z}^{\text{opt}}(0), t^{\text{opt}}(0)\}$ satisfies the constraint of problem (65), then it is the optimal solution, otherwise, the optimal dual variable $\tilde{\mu}^{\text{opt}}$ satisfies $t(\tilde{\mu}) = -\tilde{x}_f^2+2\tilde{x}_f\tilde{x}(\tilde{\mu})+L^2-2\tilde{x}(\tilde{\mu})L-\tilde{y}_f^2+2\tilde{y}_f\tilde{y}(\tilde{\mu})-\tilde{z}_f^2+2\tilde{z}_f\tilde{z}(\tilde{\mu})$. If $\tilde{z}^{\text{opt}} = z_{\min}$, the optimal solution of $\tilde{\mu}$ is the same as that in the 2D case with H^2 replaced by $-\tilde{z}_f^2+2\tilde{z}_f z_{\min}$. On the other hand, if $\tilde{z}^{\text{opt}}(\tilde{\mu}) = \frac{\delta z-\omega_z+2\tilde{\mu}\tilde{z}_f}{2a+\delta}$, then we have $\tilde{\mu}^{\text{opt}} = \left(-b_{\tilde{\mu}}^{\text{3D}}+\sqrt{(b_{\tilde{\mu}}^{\text{3D}})^2-4a_{\tilde{\mu}}^{\text{3D}}c_{\tilde{\mu}}^{\text{3D}}}\right)/(2a_{\tilde{\mu}}^{\text{3D}})$, where $a_{\tilde{\mu}}^{\text{3D}} = \frac{4(\tilde{x}_f-L)^2+4\tilde{y}_f^2+4\tilde{z}_f^2}{2a+\delta}$, $b_{\tilde{\mu}}^{\text{3D}} = \frac{\sigma^2 a_{\tilde{\mu}}^{\text{3D}}}{\sigma^2 t_f+\gamma_0 p}+d_{\tilde{\mu}}^{\text{3D}}$, $c_{\tilde{\mu}}^{\text{3D}} = \frac{\sigma^2 d_{\tilde{\mu}}^{\text{3D}}}{\sigma^2 t_f+\gamma_0 p}-1$ and $d_{\tilde{\mu}}^{\text{3D}} = -\tilde{x}_f^2-\tilde{y}_f^2-\tilde{z}_f^2+L^2+\frac{\gamma_0(1-\rho)p}{\sigma^2}+\frac{2(\tilde{x}_f-L)(\delta x-\omega_x)+2\tilde{y}_f(\delta y-\omega_y)+2\tilde{z}_f(\delta z-\omega_z)}{2a+\delta}$. By comparing the objective values achieved by these two cases, we can solve the 3D version of problem (54) efficiently. The details of the other optimization steps are not elaborated here for brevity.

To summarize, we can conclude that the proposed low-complexity algorithm can be easily extended to the case of 3D trajectory design and its convergence can also be guaranteed in the 3D case similar to the analysis in Proposition 1.

IV. Simulation results

In this section, we provide numerical results to evaluate the performance of our proposed low-complexity algorithm (i.e., Algorithm 3). For comparison, we also provide the performance of the following three benchmark schemes:

- The fixed trajectory (FT) scheme: the transmit power levels and power splitting ratios are jointly optimized, while the UAV is assumed to fly from (x_1, y_1) to (x_T, y_T) straightly at a constant speed.
- The naive power splitting (NPS) scheme: running Algorithm 3 with fixed $\rho[i] = 0.5,\ \forall i$.
- The without AN scheme: running Algorithm 3 with fixed $\rho[i] = 1,\ \forall i$.

In our simulations, the channel bandwidth, the noise power spectrum and the channel power gain are set to 20 MHz, $N_0 = -169$ dBm/Hz and $\gamma_0 = -36$ dB, respectively, and the carrier frequency is set at 5 GHz. Hence, the reference SNR at a distance of 1 m is $\frac{\gamma_0}{\sigma^2} = 60$ dB. The nominal system configuration is defined by the following choice of parameters unless otherwise specified: $L = 100$ m, $H = 100$ m, $V_{\max} = 12$ m/s, $M = 4$ kg, $N = 125$ s, $\delta_t = 0.5$ s, $(x_1, y_1) = (-200\text{ m}, -150\text{ m})$, $(x_T, y_T) = (1000\text{ m}, -150\text{ m})$, $\bar{P} = 0$ dBm and $P_{\max} = 4\bar{P}$. The total mobility energy stored at the UAV E_{tr} is set to 19.40 kJ. The simulations are implemented in MATLAB R2016b and carried out on a workstation with Intel Xeon(R) CPU E5-2640 running at 2.6 GHz and with 128 GB RAM.

1) Convergence property: First, we illustrate in Fig. 3 the convergence of our proposed Algorithm 2 and 3. From Fig. 3 (a), it is observed that the outer BCD iteration of Algorithm 3 is monotonically convergent and it needs about 10 iterations to obtain the steady performance. Besides, in Fig. 3 (b) and (c), we plot the primal and dual residuals $\|\mathbf{r}\|$ and $\|\mathbf{s}\|$ versus the number of ADMM iterations in Algorithm 2. As can be seen, Algorithm 2 can converge well within 2000 iterations. Although this number is relatively large as compared with the number of outer BCD iterations, the complexity is low since each updating step in Algorithm 2 is very simple, this will be verified in the following results.

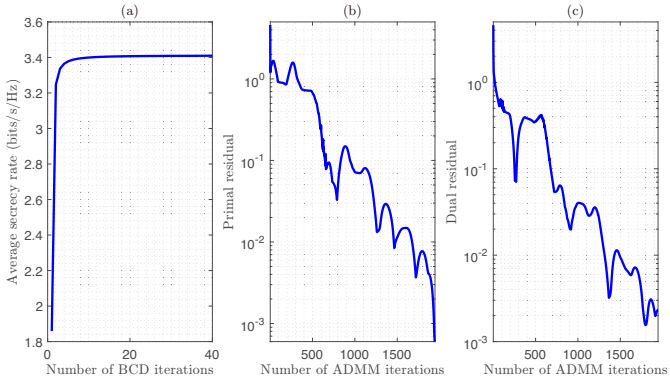

Fig. 3: Convergence behavior of the proposed Algorithm 2 and 3.

2) Performance and complexity: In Fig. 4 and Table I, we respectively investigate the average running time required by Algorithm 3 to complete one outer BCD iteration and the achieved objective value (i.e., the average secrecy rate) in bits/s/Hz by Algorithm 3. For comparison, we also provide the performance achieved by replacing Algorithm 1 and 2 in steps 3 and 4 of Algorithm 3 by using the CVX solver [32]. From Fig. 4, we observe that the running time required by the proposed algorithm is significantly less than that required by using CVX. The running time increases with the increasing of T, however, it increases much slower for the proposed algorithm. This is consistent with the complexity analysis in Section III-C and it shows that the proposed algorithm design is more scalable. Besides, we observe from Table I that the average secrecy rate achieved by the proposed algorithm and that by CVX is almost identical. In certain cases, such as $T = 240$, the performance of the proposed algorithm is even better. This is because the CVX solver uses a successive approximation heuristic method to solve convex optimization problems involving $\log(\cdot)$ functions, which may lead to certain performance loss due to precision issues.

TABLE I: Achieved Average Secrecy Rate Comparison

	Numbers of time slots T					
	200	220	240	260	280	300
Using CVX	2.2019	2.9532	3.2711	3.5375	3.7640	3.9580
Algorithm 3	2.2019	2.9532	3.2721	3.5375	3.7640	3.9580

3) Average secrecy rate versus the Bob-Eve distance L: In Fig. 5, we plot the average secrecy rates achieved by the considered schemes under various values of L. First, it is observed that the proposed algorithm achieves the best performance among the considered schemes. Second, the achieved average secrecy rates by all the considered schemes increases with L, which is expected since it is more difficult for Eve to intercept the communications between Bob and the UAV when L is large. Similarly, since transmitting AN is less important under larger L, the performance of the without AN scheme approaches that of the proposed algorithm with the increasing of L. Besides, we observe that the performance of the NPS scheme is better than that of the FT scheme. This is due to the fact that optimizing the UAV's trajectory under the considered simulation setup enables the UAV to fly close to Bob and away from Eve to achieve higher secrecy rate, while the performance gain offered by optimizing the power splitting ratios $\{\rho[i]\}$ is not that pronounced.

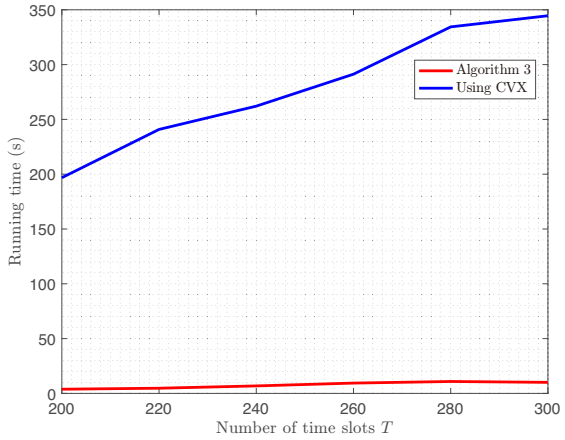

Fig. 4: Running time comparison.

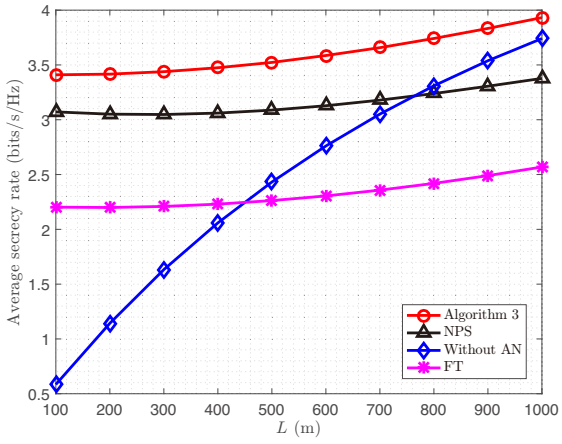

Fig. 5: Average secrecy rate versus L.

4) Average secrecy rate versus the total flight time N: In Fig. 6, we investigate the average secrecy rate versus various values of N. As can be seen, the performance of all the considered schemes improves with the increasing of N, except for the FT scheme. This is because with increasingly large T, the UAV is able to hover over its favorable locations for a longer time, which leads to higher secrecy rate. However, if the

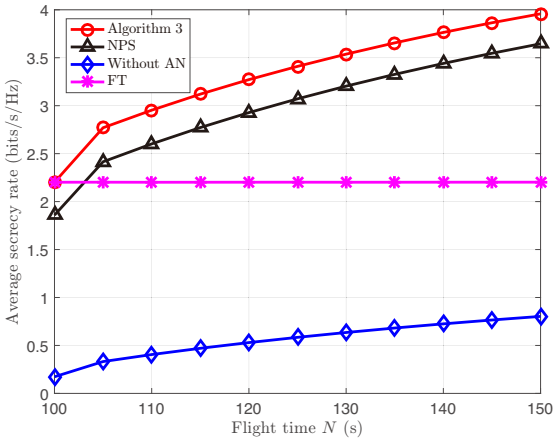

Fig. 6: Average secrecy rate versus N.

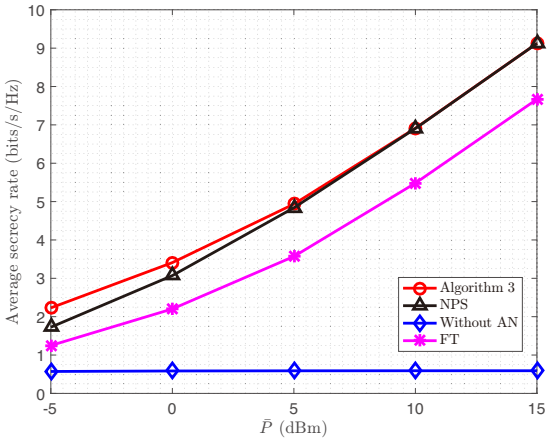

Fig. 7: Average secrecy rate versus $\bar{P}$.

mobility of the UAV cannot be exploited as in the FT scheme, the achieved average secrecy rate will remain unchanged even for sufficiently large N. Besides, we can observe that when N is small (e.g., $N = 100$ s), the performance of the FT scheme is better than that of the NPS scheme, since in this case, the advantage of mobility control cannot be exploited due to the limited flight time. Moreover, the proposed Algorithm 3 outperforms the other analyzed schemes.

5) Average secrecy rate versus the average transmit power $\bar{P}$: Fig. 7 plots the average secrecy rates of different schemes versus $\bar{P}$. As shown, the proposed Algorithm 3 always achieves the highest average secrecy rate, while the without AN scheme provides the lowest average secrecy rate. The performance achieved by the proposed scheme, the FT scheme and the NPS scheme all improves with the increasing of $\bar{P}$, while that by the without AN scheme does not change much. This is because the Bob-Eve distance is set to $L = 100$ m, which is relatively close and thus the qualities of the UAB-Bob and UAV-Eve links both improve as $\bar{P}$ increases since no AN is available to degrade the UAV-Eve link. Besides, we observe that the performance gain of the proposed algorithm over the NPS scheme gradually decreases and approaches zero as $\bar{P}$ increases. This is reasonable since the achievable rates of the UAV-Bob and UAV-Eve links are $\log(\cdot)$ functions of $\{\text{SNR}_\text{I}[i]\}$ and $\{\text{SINR}_\text{E}[i]\}$, they tend to gradually saturate as $\bar{P}$ increases, which will limit the gain offered by the power splitting.

6) Trajectories under various values of E_{th}: Fig. 8 shows the trajectories of the UAV by employing different schemes when $E_\text{th} = 14.55$ kJ and $E_\text{th} = 19.40$ kJ. First, we can see that with larger E_th, the UAV can fly closer to Bob to achieve a higher secrecy rate and this holds for all the considered schemes. Second, it is observed that the trajectories of the proposed algorithm and the without AN scheme differ significantly with $E_\text{th} = 14.55$ kJ or $E_\text{th} = 19.40$ kJ, especially when the UAV flies towards Bob. Specifically, with the ability to transmit AN (in the proposed algorithm and the NPS scheme), the UAV can fly closer to Bob and Eve, while for the without AN scheme, the UAV has to keep a certain distance away from Bob in order to weaken the UAV-Eve link. Besides, the trajectories of the proposed algorithm and the NPS scheme are almost identical, which implies that the UAV's trajectory is not sensitive to the power splitting ratios under the considered simulation setups.

7) Trajectories under various values of N: In Fig. 9, we show the trajectories of the UAV by employing different schemes when $N = 103$ s and $N = 125$ s. We observe that when the flight time is long enough (i.e., $N = 125$ s), the UAV can fly close to Bob and Eve, while when $N = 103$ s, the UAV has to head back to the final location before it can reach its most favorable location. Besides, similar to the results in Fig. 8, the trajectories of the proposed algorithm and the without AN scheme are different owing to the difference in the ability of transmitting AN signals.

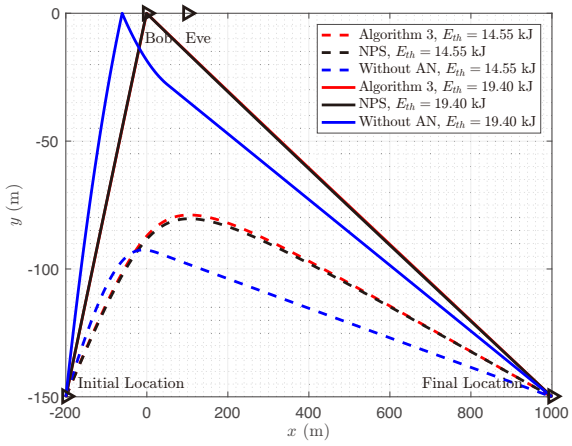

Fig. 8: Trajectories of the UAV under various values of E_th.

V. Conclusion

In this work, we proposed a power splitting approach to secure the UAV communication against a potential ground Eve, by enabling the UAV to transmit confidential information and AN simultaneously. By exploiting the power splitting capability of the UAV and its controllable mobility, we maximized the average secrecy rate by jointly optimizing the

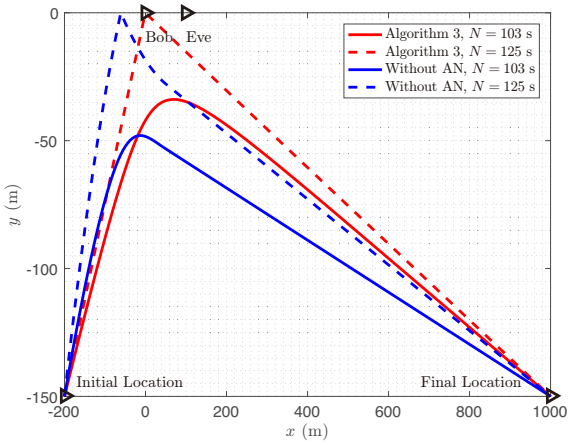

Fig. 9: Trajectories of UAV using different algorithms.

UAVs trajectory, the transmit power levels and the power splitting ratios over time. An iterative algorithm with very low complexity was proposed to solve the considered optimization problem with guaranteed convergence. Numerical results showed the effectiveness of our proposed algorithm. It is worth noting that the proposed algorithm and the underlying techniques that are employed can be extended to other joint power and trajectory optimization problems for UAV-enabled communication systems.

Appendix A
Brief Introduction to ADMM

To illustrate the idea of the ADMM, let us consider the following convex optimization problem:

$$\min_{\mathbf{x}\in\mathbb{R}^{n\times 1},\ \mathbf{z}\in\mathbb{R}^{m\times 1}} f(\mathbf{x})+g(\mathbf{z}) \quad \text{s.t. } \mathbf{A}\mathbf{x}+\mathbf{B}\mathbf{z}=\mathbf{c},\ \mathbf{x}\in\mathcal{C}_1,\ \mathbf{z}\in\mathcal{C}_2, \tag{66}$$

where $f(\cdot):\mathbb{R}^{n\times 1}\mapsto\mathbb{R}$ and $g(\cdot):\mathbb{R}^{m\times 1}\mapsto\mathbb{R}$ are convex functions, $\mathcal{C}_1\in\mathbb{R}^{n\times 1}$ and $\mathcal{C}_2\in\mathbb{R}^{m\times 1}$ are non-empty convex sets, $\mathbf{A}\in\mathbb{R}^{p\times n},\mathbf{B}\in\mathbb{R}^{p\times m},\mathbf{c}\in\mathbb{R}^{p\times 1}$. Assume that problem (66) is feasible and strong duality holds.

The ADMM solves problem (66) by resorting to the following AL problem:

$$\min_{\mathbf{x}\in\mathbb{R}^{n\times 1},\ \mathbf{z}\in\mathbb{R}^{m\times 1}} L_\rho(\mathbf{x},\mathbf{z},\boldsymbol{\lambda}) \quad \text{s.t. } \mathbf{x}\in\mathcal{C}_1,\ \mathbf{z}\in\mathcal{C}_2, \tag{67}$$

where $L_\rho(\mathbf{x},\mathbf{z},\boldsymbol{\lambda})=f(\mathbf{x})+g(\mathbf{z})+\boldsymbol{\lambda}^T(\mathbf{A}\mathbf{x}+\mathbf{B}\mathbf{z}-\mathbf{c})+\frac{\rho}{2}\|\mathbf{A}\mathbf{x}+\mathbf{B}\mathbf{z}-\mathbf{c}\|^2$, $\boldsymbol{\lambda}$ denotes the dual variable and ρ is the penalty parameter. Then, the ADMM iterates over the following three steps:

$$\mathbf{x}_{k+1}=\arg\min_{\mathbf{x}\in\mathbb{R}^{n\times 1}} L_\rho(\mathbf{x},\mathbf{z}_k,\boldsymbol{\lambda}_k), \tag{68a}$$

$$\mathbf{z}_{k+1}=\arg\min_{\mathbf{z}\in\mathbb{R}^{m\times 1}} L_\rho(\mathbf{x}_{k+1},\mathbf{z},\boldsymbol{\lambda}_k), \tag{68b}$$

$$\boldsymbol{\lambda}_{k+1}=\boldsymbol{\lambda}_k+\rho(\mathbf{A}\mathbf{x}_{k+1}+\mathbf{B}\mathbf{z}_{k+1}-\mathbf{c}), \tag{68c}$$

where k denotes the iteration index. The convergence criterion of the ADMM can be expressed as $\|\mathbf{r}_{k+1}\|\le\epsilon$ and $\|\mathbf{s}_{k+1}\|\le\epsilon$, where $\mathbf{r}_{k+1}$ and $\mathbf{s}_{k+1}$ denote the primal residual and dual residual in the $(k+1)$-th iteration, which are defined as

$$\begin{aligned}\mathbf{r}_{k+1}&=\mathbf{A}\mathbf{x}_{k+1}+\mathbf{B}\mathbf{z}_{k+1}-\mathbf{c},\\ \mathbf{s}_{k+1}&=\rho\mathbf{A}^T\mathbf{B}(\mathbf{z}_{k+1}-\mathbf{z}_k).\end{aligned} \tag{69}$$

It can be seen that the ADMM alternately performs one iteration of primal variables updates, i.e., (68a) and (68b), and one step of outer subgradient update for the dual variable, i.e., (68c). It converges to the global optimum of problem (66) under relatively loose conditions, for two-block convex separable problems. For more details, please refer to [49].

Appendix B
Optimal Solution to Problem (53)

It can be readily seen that problem (53) is convex and strong duality holds, therefore, it can be solved by resorting to the dual problem. Specifically, the Lagrangian function of problem (53) is given by $L_1=L_{\delta,1}-\mu((x[2i]-\bar{x}[2i+1])^2+(y[2i]-\bar{y}[2i+1])^2-V_{\max}^2\delta_t^2)$, where μ denotes the Lagrangian multiplier. Then, by setting $\frac{\partial L_1}{\partial\bar{x}[2i+1]}=0$, we have

$$\bar{x}^{\text{opt}}[2i+1]=\frac{1}{2\mu+\delta}(2\mu x[2i]+\delta x[2i+1]-\lambda_{x_{2i+1}}). \tag{70}$$

Substituting (70) into L_1 and taking the partial derivative of L_1 with respect to $x[2i]$, we can obtain

$$\begin{aligned}&-\delta\big(x[2i]-\bar{x}[2i]-\frac{\lambda_{x_{2i}}}{\delta}+x[2i]-\hat{x}[2i]-\frac{\eta_{x_{2i}}}{\delta}+x[2i]\\&-\tilde{x}[2i]-\frac{\omega_{x_{2i}}}{\delta}\big)-\frac{2\mu\delta}{2\mu+\delta}\big(x[2i]-x[2x+1]+\frac{\lambda_{x_{2i+1}}}{\delta}\big)=0.\end{aligned} \tag{71}$$

Based on (71), the optimal $x^{\text{opt}}[2i]$ can be expressed as

$$\begin{aligned}x^{\text{opt}}[2i]=&\frac{1}{3\delta+\frac{2\mu\delta}{2\mu+\delta}}\Big(\delta(\bar{x}[2i]+\hat{x}[2i]+\tilde{x}[2i])+\lambda_{x_{2i}}\\&+\eta_{x_{2i}}+\omega_{x_{2i}}+\frac{2\mu\delta}{2\mu+\delta}(x[2i+1]-\frac{\lambda_{x_{2i+1}}}{\delta})\Big).\end{aligned} \tag{72}$$

Similarly, we have

$$\bar{y}^{\text{opt}}[2i+1]=(2\mu y[2i]+\delta y[2i+1]-\lambda_{y_{2i+1}})/(2\mu+\delta), \tag{73}$$

and

$$\begin{aligned}y^{\text{opt}}[2i]=&\frac{1}{3\delta+\frac{2\mu\delta}{2\mu+\delta}}\Big(\delta(\bar{y}[2i]+\hat{y}[2i]+\tilde{y}[2i])+\lambda_{y_{2i}}\\&+\eta_{y_{2i}}+\omega_{y_{2i}}+\frac{2\mu\delta}{2\mu+\delta}(y[2i+1]-\frac{\lambda_{y_{2i+1}}}{\delta})\Big).\end{aligned} \tag{74}$$

Then, it is not difficult to see that if $\bar{x}^{\text{opt}}[2i+1]$, $x^{\text{opt}}[2i]$, $\bar{y}^{\text{opt}}[2i+1]$ and $y^{\text{opt}}[2i]$ satisfy $(x^{\text{opt}}[2i]-\bar{x}^{\text{opt}}[2i+1])^2+(y^{\text{opt}}[2i]-\bar{y}^{\text{opt}}[2i+1])^2\le V_{\max}^2\delta_t^2$ when $\mu=0$, then this is the optimal solution. Otherwise, we substitute (70), (72), (73) and (74) into $(x[2i]-\bar{x}[2i+1])^2+(y[2i]-\bar{y}[2i+1])^2=V_{\max}^2\delta_t^2$

(due to the complementary slackness). By solving this equation with respect to μ, we have $\mu^{\text{opt}} = (\sqrt{A} - 3\delta^2)/(8\delta)$, where

$$\begin{aligned} A =& \frac{\delta^2}{V_{\max}^2 \delta_t^2} \Big(\big(\delta(\hat{x}[2i] + \tilde{x}[2i] + \bar{x}[2i]) + \omega_{x_{2i}} + \eta_{x_{2i}} \\ &+ \lambda_{x_{2i}} + 3\lambda_{x_{2i+1}} - 3\delta x[2i+1]\big)^2 \\ &+ \big(\delta(\hat{y}[2i] + \tilde{y}[2i] + \bar{y}[2i]) + \omega_{y_{2i}} + \eta_{y_{2i}} \\ &+ \lambda_{y_{2i}} + 3\lambda_{y_{2i+1}} - 3\delta y[2i+1]\big)^2 \Big). \end{aligned} \tag{75}$$

Substituting μ^{opt} back into (70), (72), (73) and (74), we can obtain the optimal solution of problem (53).

Appendix C
Optimal Solution to Problem (54)

For notational simplicity, in this appendix, we ignore the time slot index $2i+1$ in the variables $\{\tilde{x}[2i+1], \tilde{y}[2i+1], x[2i+1], y[2i+1], u[2i+1], t[2i+1], \rho[2i+1], p[2i+1], \omega_{x_{2i+1}}, \omega_{y_{2i+1}}\}$ without loss of generality. First, we can observe that $L_{\delta,2}$ is a decreasing function with respect to u, therefore the optimal u, denoted as u^{opt}, must satisfy $u^{\text{opt}} = \tilde{x}^2 + \tilde{y}^2 + H^2$. By substituting u^{opt} into $L_{\delta,2}$, we obtain $L_{\delta,2} = -a(\tilde{x}^2 + \tilde{y}^2 + H^2) - \frac{\sigma^2 t}{t_f + \gamma_0 p} + \log(\gamma_0(1-\rho)p + \sigma^2 t) - \frac{\delta}{2}\big((x - \tilde{x} - \frac{\omega_x}{\delta})^2 + (y - \tilde{y} - \frac{\omega_y}{\delta})^2\big)$. Hence, problem (54) becomes

$$\begin{aligned} &\max_{\tilde{x},\, \tilde{y},\, t} \; L_{\delta,2} \\ &\text{s.t. } t \le -\tilde{x}_f^2 + 2\tilde{x}_f\tilde{x} + L^2 - 2\tilde{x}L - \tilde{y}_f^2 + 2\tilde{y}_f\tilde{y} + H^2. \end{aligned} \tag{76}$$

Since problem (76) is convex, we can globally solve it by resorting to its dual problem. The corresponding Lagrange function for problem (76) can be expressed as $L_{\delta,2,\tilde{\mu}} \triangleq L_{\delta,2} - \tilde{\mu}\big(t + \tilde{x}_f^2 - 2(\tilde{x}_f - L)\tilde{x} - L^2 + \tilde{y}_f^2 - 2\tilde{y}_f\tilde{y} - H^2\big)$, where $\tilde{\mu}$ is the dual variable.

By checking the first-order optimality condition, we can express the optimal solution of problem (76) as a function of $\tilde{\mu}$, i.e.,

$$\begin{aligned} \tilde{x}^{\text{opt}}(\tilde{\mu}) &= \frac{\delta x - \omega_x + 2\tilde{\mu}(\tilde{x}_f - L)}{2a + \delta}, \\ \tilde{y}^{\text{opt}}(\tilde{\mu}) &= \frac{\delta y - \omega_y + 2\tilde{\mu}\tilde{y}_f}{2a + \delta}, \\ t^{\text{opt}}(\tilde{\mu}) &= \frac{\sigma^2 t_f + \gamma_0 p}{\tilde{\mu}(\sigma^2 t_f + \gamma_0 p) + \sigma^2} - \frac{\gamma_0(1-\rho)p}{\sigma^2}. \end{aligned} \tag{77}$$

If the solution $\{\tilde{x}^{\text{opt}}(0), \tilde{y}^{\text{opt}}(0), t^{\text{opt}}(0)\}$ automatically satisfies the constraint of problem (76), then it is the optimal solution, otherwise, we can see that the optimal dual variable $\tilde{\mu}^{\text{opt}}$ satisfies

$$\begin{aligned} t^{\text{opt}}(\tilde{\mu}^{\text{opt}}) =& -\tilde{x}_f^2 + 2(\tilde{x}_f - L)\tilde{x}^{\text{opt}}(\tilde{\mu}^{\text{opt}}) \\ &+ L^2 - \tilde{y}_f^2 + 2\tilde{y}_f\tilde{y}^{\text{opt}}(\tilde{\mu}^{\text{opt}}) + H^2. \end{aligned} \tag{78}$$

Substituting (77) into (78) and solving the resulting quadratic equation, we obtain $\tilde{\mu}^{\text{opt}} = \Big(-b_{\tilde{\mu}} + \sqrt{b_{\tilde{\mu}}^2 - 4a_{\tilde{\mu}}c_{\tilde{\mu}}}\Big)/(2a_{\tilde{\mu}})$, where $a_{\tilde{\mu}} = \frac{4(\tilde{x}_f - L)^2 + 4\tilde{y}_f^2}{2a+\delta}$, $b_{\tilde{\mu}} = \frac{\sigma^2 a_{\tilde{\mu}}}{\sigma^2 t_f + \gamma_0 p} + d_{\tilde{\mu}}$, $c_{\tilde{\mu}} = \frac{\sigma^2 d_{\tilde{\mu}}}{\sigma^2 t_f + \gamma_0 p} - 1$ and $d_{\tilde{\mu}} = -\tilde{x}_f^2 - \tilde{y}_f^2 + L^2 + H^2 + \frac{\gamma_0(1-\rho)p}{\sigma^2} + \frac{2(\tilde{x}_f - L)(\delta x - \omega_x) + 2\tilde{y}_f(\delta y - \omega_y)}{2a+\delta}$.

Appendix D
Optimal Solution to Problem (55)

The Lagrangian function of problem (55) can be expressed as $L_3 = L_{\delta,3} - \phi \sum_{i=1}^{T-1} ((\ddot{x}[i] - \ddot{x}[i+1])^2 + (\ddot{y}[i] - \ddot{y}[i+1])^2) + \phi \frac{E_{\text{tr}}}{\kappa}$. By setting $\frac{\partial L_{\delta,3}}{\partial \hat{x}[2i+1]} = 0$ and $\frac{\partial L_{\delta,3}}{\partial \hat{y}[2i+1]} = 0$, we have

$$\hat{x}^{\text{opt}}[2i+1] = \frac{1}{2}\Big(\ddot{x}[2i+1] + \frac{\theta_{x_{2i+1}}}{\delta} + x[2i+1] - \frac{\eta_{x_{2i+1}}}{\delta}\Big), \tag{79}$$

$$\hat{y}^{\text{opt}}[2i+1] = \frac{1}{2}\Big(\ddot{y}[2i+1] + \frac{\theta_{y_{2i+1}}}{\delta} + y[2i+1] - \frac{\eta_{y_{2i+1}}}{\delta}\Big). \tag{80}$$

Substituting (79) and (80) into L_3 and letting $\frac{\partial L_3}{\partial \ddot{x}[2i+1]} = 0$ and $\frac{\partial L_3}{\partial \ddot{x}[2i]} = 0$, we can obtain the following equations:

$$\begin{aligned} &\Big(-4\phi - \frac{\delta}{2}\Big)\ddot{x}[2i+1] + 2\phi(\ddot{x}[2i+2] + \ddot{x}[2i]) \\ &\quad + \frac{\delta}{2}\left(x[2i+1] - \frac{\eta_{x_{2i+1}} + \theta_{x_{2i+1}}}{\delta}\right) = 0, \end{aligned} \tag{81}$$

$$-(\delta + 4\phi)\ddot{x}[2i] + \delta\hat{x}[2i] - \theta_{x_{2i}} + 2\phi(\ddot{x}[2i+1] + \ddot{x}[2i+1]) = 0. \tag{82}$$

Similarly, for $\ddot{y}[2i+1]$ and $\ddot{y}[2i]$, we have

$$\begin{aligned} &\Big(-4\phi - \frac{\delta}{2}\Big)\ddot{y}[2i+1] + 2\phi(\ddot{y}[2i+2] + \ddot{y}[2i]) \\ &\quad + \frac{\delta}{2}\left(y[2i+1] - \frac{\eta_{y_{2i+1}} + \theta_{y_{2i+1}}}{\delta}\right) = 0, \end{aligned} \tag{83}$$

$$-(\delta + 4\phi)\ddot{y}[2i] + \delta\hat{y}[2i] - \theta_{y_{2i}} + 2\phi(\ddot{y}[2i+1] + \ddot{y}[2i+1]) = 0. \tag{84}$$

Together with $\ddot{x}[1] = x_1$, $\ddot{x}[T] = x_T$, $\ddot{y}[1] = y_1$ and $\ddot{y}[T] = y_T$, we can employ the Gaussian elimination [50] (a celebrated algorithm in linear algebra for solving a system of linear equations) to solve the above equations for a given dual variable ϕ and the optimal ϕ can be found by using the Bisection method.

Appendix E
Proof of Proposition 2

Let $g_i^{\text{3D}}(x[i], y[i], z[i], p[i], \rho[i]) \triangleq \log\Big(1 + \frac{\gamma_0 a[i]}{d_{\text{I3}}^2[i]\sigma^2}\Big) - \log\Big(1 + \frac{\gamma_0 a[i]}{\gamma_0 b[i] + \sigma^2 d_{\text{E3}}^2[i]}\Big)$ (recall that $a[i] = p[i]\rho[i]$ and $b[i] = p[i](1-\rho[i])$ as defined in (19)), then by taking the partial derivative of $g_i^{\text{3D}}(x[i], y[i], z[i], p[i], \rho[i])$ with respect to $z[i]$, we have[6]

$$\frac{\partial g_i^{\text{3D}}}{\partial z[i]} = \begin{cases} 2z[i](f(d_{\text{I3}}[i]^2) - f(\frac{\gamma_0 b[i]}{\sigma^2} + d_{\text{E3}}[i]^2)), \text{ if } g_i^{\text{3D}} \ge 0, \\ 0, \text{ otherwise.} \end{cases} \tag{85}$$

where $f(x) \triangleq \frac{1}{\gamma_0 a[i]/\sigma^2 + x} - \frac{1}{x}$. Note that $f(x)$ is a monotonically increasing function since $\frac{\partial f(x)}{\partial x} = -\frac{1}{(\gamma_0 a[i]/\sigma^2 + x)^2} + \frac{1}{x^2} > 0$. Besides, we have $d_{\text{I3}}[i]^2 < \gamma_0 b/\sigma^2 + d_{\text{E3}}[i]^2$ when $g_i^{\text{3D}} > 0$. Therefore, $\frac{\partial g_i^{\text{3D}}}{\partial z[i]}$ satisfies $\frac{\partial g_i^{\text{3D}}}{\partial z[i]} < 0$, if $g_i^{\text{3D}} > 0$, and $\frac{\partial g_i^{\text{3D}}}{\partial z[i]} = 0$ otherwise. This implies that $\frac{\partial g_i^{\text{3D}}}{\partial z[i]} \le 0$ is always satisfied, which means that g_i^{3D} will decrease or remain unchanged with the increasing of $z[i]$. Thus, we can see that (60) holds, which completes the proof.

[6] In the following, $g_i^{\text{3D}}(x[i], y[i], z[i], p[i], \rho[i])$ is abbreviated as g_i^{3D} for notational simplicity.

REFERENCES

[1] Y. Zeng, R. Zhang, and T. J. Lim, "Wireless communications with unmanned aerial vehicles: Opportunities and challenges," *IEEE Commun. Mag.*, vol. 54, no. 5, pp. 36–42, May 2016.

[2] Y. Cai, F. Cui, Q. Shi, M. J. Zhao, and G. Y. Li, "Dual-UAV-enabled secure communications: Joint trajectory design and user scheduling," *IEEE J. Sel. Areas Commun.*, vol. 36, no. 9, pp. 1972–1985, Sep. 2018.

[3] X. Sun, D. W. K. Ng, Z. Ding, Y. Xu, and Z. Zhong, "Physical layer security in UAV systems: Challenges and opportunities," *IEEE Wireless Commun.*, vol. 26, no. 5, pp. 40–47, Oct. 2019.

[4] M. M. Zhao, Q. Shi, and M. J. Zhao, "Efficiency maximization for UAV-enabled mobile relaying systems with laser charging," *IEEE Trans. Wireless Commun.*, vol. 19, no. 5, pp. 3257–3272, May 2020.

[5] "Ericsson and China Mobile conduct worlds first 5G drone prototype field trial," [Online]. Available: https://www.ericsson.com/en/news/2016/8/ericsson-and-china-mobileconduct- worlds-first-5g-drone-prototype-field-trial-.

[6] Y. Zeng, Q. Wu, and R. Zhang, "Accessing from the sky: A tutorial on UAV communications for 5G and beyond," *Proc. IEEE*, vol. 107, no. 12, pp. 2327–2375, Dec. 2019.

[7] J. Zhang, T. Chen, S. Zhong, J. Wang, W. Zhang, X. Zuo, R. G. Maunder, and L. Hanzo, "Aeronautical $ad\ hoc$ networking for the internet-above-the-clouds," *Proc. IEEE*, vol. 107, no. 5, pp. 868–911, May 2019.

[8] C. Xu, T. Bai, J. Zhang, R. Rajashekar, R. G. Maunder, Z. Wang, and L. Hanzo, "Adaptive coherent/non-coherent spatial modulation aided unmanned aircraft systems," *IEEE Wireless Commun.*, vol. 26, no. 4, pp. 170–177, Aug. 2019.

[9] S. Zhang, Y. Zeng, and R. Zhang, "Cellular-enabled UAV communication: A connectivity-constrained trajectory optimization perspective," *IEEE Trans. Commun.*, vol. 67, no. 3, pp. 2580–2604, Mar. 2019.

[10] 3GPP, "Technical specification group radio access network: Study on enhanced LTE support for aerial vehicles," TR 36.777, v. 15.0.0, 2017.

[11] Y. Liang, H. V. Poor, and S. Shamai, "Secure communication over fading channels," *IEEE Trans. Inf. Theory*, vol. 54, no. 6, pp. 2470–2492, Jun. 2008.

[12] Q. Wu, W. Mei, and R. Zhang, "Safeguarding wireless network with UAVs: A physical layer security perspective," *IEEE Wireless Commun.*, vol. 26, no. 5, pp. 12–18, Oct. 2019.

[13] L. Xiao, C. Xie, M. Min, and W. Zhuang, "User-centric view of unmanned aerial vehicle transmission against smart attacks," *IEEE Trans. Veh. Technol.*, vol. 67, no. 4, pp. 3420–3430, Apr. 2018.

[14] G. Zhang, Q. Wu, M. Cui, and R. Zhang, "Securing UAV communications via joint trajectory and power control," *IEEE Trans. Wireless Commun.*, vol. 18, no. 2, pp. 1376–1389, Feb. 2019.

[15] Z. Li, M. Chen, C. Pan, N. Huang, Z. Yang, and A. Nallanathan, "Joint trajectory and communication design for secure UAV networks," *IEEE Commun. Lett.*, vol. 23, no. 4, pp. 636–639, Apr. 2019.

[16] J. Yao and J. Xu, "Joint 3D maneuver and power adaptation for secure UAV communication with CoMP reception," *IEEE Trans. Wireless Commun.*, DOI: 10.1109/TWC.2020.3007648, Jul. 2020.

[17] H. Wu, Y. Wen, J. Zhang, Z. Wei, N. Zhang, and X. Tao, "Energy-efficient and secure air-to-ground communication with jittering UAV," *IEEE Trans. Veh. Technol.*, vol. 69, no. 4, pp. 3954–3967, Apr. 2020.

[18] Y. Zhou, C. Pan, P. L. Yeoh, K. Wang, M. Elkashlan, B. Vucetic, and Y. Li, "Secure communications for UAV-enabled mobile edge computing systems," *IEEE Trans. Commun.*, vol. 68, no. 1, pp. 376–388, Jan. 2020.

[19] Q. Wang, Z. Chen, W. Mei, and J. Fang, "Improving physical layer security using UAV-enabled mobile relaying," *IEEE Wireless Commun. Lett.*, vol. 6, no. 3, pp. 310–313, Jun. 2017.

[20] Y. Zhou, P. L. Yeoh, H. Chen, Y. Li, R. Schober, L. Zhuo, and B. Vucetic, "Improving physical layer security via a UAV friendly jammer for unknown eavesdropper location," *IEEE Trans. Veh. Technol.*, vol. 67, no. 11, pp. 11 280–11 284, Nov. 2018.

[21] A. Li, Q. Wu, and R. Zhang, "UAV-enabled cooperative jamming for improving secrecy of ground wiretap channel," *IEEE Wireless Commun. Lett.*, vol. 8, no. 1, pp. 181–184, Feb. 2019.

[22] M. Hua, Y. Wang, Q. Wu, H. Dai, Y. Huang, and L. Yang, "Energy-efficient cooperative secure transmission in multi-UAV-enabled wireless networks," *IEEE Trans. Veh. Technol.*, vol. 68, no. 8, pp. 7761–7775, Aug. 2019.

[23] Y. Chen and Z. Zhang, "UAV-aided secure transmission in MISOME wiretap channels with imperfect CSI," *IEEE Access*, vol. 7, pp. 98 107–98 121, 2019.

[24] C. Zhong, J. Yao, and J. Xu, "Secure UAV communication with cooperative jamming and trajectory control," *IEEE Commun. Lett.*, vol. 23, no. 2, pp. 286–289, Feb. 2019.

[25] J. P. Vilela, M. Bloch, J. Barros, and S. W. McLaughlin, "Wireless secrecy regions with friendly jamming," *IEEE Trans. Inf. Forens. Sec.*, vol. 6, no. 2, pp. 256–266, Jun. 2011.

[26] S. Goel and R. Negi, "Guaranteeing secrecy using artificial noise," *IEEE Trans. Wireless Commun.*, vol. 7, no. 6, pp. 2180–2189, Jun. 2008.

[27] X. Zhou and M. R. McKay, "Secure transmission with artificial noise over fading channels: Achievable rate and optimal power allocation," *IEEE Trans. Veh. Technol.*, vol. 59, no. 8, pp. 3831–3842, Oct. 2010.

[28] H. Xing, L. Liu, and R. Zhang, "Secrecy wireless information and power transfer in fading wiretap channel," *IEEE Trans. Veh. Technol.*, vol. 65, no. 1, pp. 180–190, Jan. 2016.

[29] A. Beck and L. Tetruashvili, "On the convergence of block coordinate descent type methods," *SIAM journal on Optimization*, vol. 23, no. 4, pp. 2037–2060, 2013.

[30] G. R. Lanckriet and B. K. Sriperumbudur, "On the convergence of the concave-convex procedure," *in Advances in Neural Information Processing Systems*, pp. 1759–1767, 2009.

[31] S. Boyd, N. Parikh, E. Chu, B. Peleato, J. Eckstein *et al.*, "Distributed optimization and statistical learning via the alternating direction method of multipliers," *Foundations and Trends® in Machine learning*, vol. 3, no. 1, pp. 1–122, 2011.

[32] M. Grant and S. Boyd, "CVX: Matlab software for disciplined convex programming, version 2.1," http://cvxr.com/cvx, Mar. 2014.

[33] S. Jeong, O. Simeone, and J. Kang, "Mobile edge computing via a UAV-mounted cloudlet: Optimization of bit allocation and path planning," *IEEE Trans. Veh. Technol.*, vol. 67, no. 3, pp. 2049–2063, Mar. 2018.

[34] N. Xue, "Design and optimization of lithium-ion batteries for electricvehicle applications," Doctoral dissertation, University of Michigan, 2014.

[35] 3GPP TR 36.777, "Enhanced LTE support for aerial vehicles," ftp://www.3gpp.org/specs/archive/36_series/36.777, accessed Sep. 3, 2020.

[36] X. Lin, V. Yajnanarayana, S. D. Muruganathan, S. Gao, H. Asplund, H. Maattanen, M. Bergstrom, S. Euler, and Y. P. E. Wang, "The sky is not the limit: LTE for unmanned aerial vehicles," *IEEE Commun. Mag.*, vol. 56, no. 4, pp. 204–210, Apr. 2018.

[37] A. Al-Hourani, S. Kandeepan, and S. Lardner, "Optimal LAP altitude for maximum coverage," *IEEE Wireless Commun. Lett.*, vol. 3, no. 6, pp. 569–572, Dec. 2014.

[38] H. Ren, C. Pan, K. Wang, Y. Deng, M. Elkashlan, and A. Nallanathan, "Achievable data rate for URLLC-enabled UAV systems with 3-D channel model," *IEEE Wireless Commun. Lett.*, vol. 8, no. 6, pp. 1587–1590, Dec. 2019.

[39] H. Ren, C. Pan, K. Wang, W. Xu, M. Elkashlan, and A. Nallanathan, "Joint transmit power and placement optimization for URLLC-enabled UAV relay systems," *IEEE Trans. Veh. Technol.*, vol. 69, no. 7, pp. 8003–8007, Jul. 2020.

[40] A. A. Khuwaja, Y. Chen, N. Zhao, M. Alouini, and P. Dobbins, "A survey of channel modeling for UAV communications," *IEEE Commun. Surveys Tuts.*, vol. 20, no. 4, pp. 2804–2821, Fourthquarter 2018.

[41] S. Goel and R. Negi, "Guaranteeing secrecy using artificial noise," *IEEE Trans. Wireless Commun.*, vol. 7, no. 6, pp. 2180–2189, Jun. 2008.

[42] P. K. Gopala, L. Lai, and H. El Gamal, "On the secrecy capacity of fading channels," *IEEE Trans. Inf. Theory*, vol. 54, no. 10, pp. 4687–4698, Oct. 2008.

[43] M. M. Zhao, Y. Cai, Q. Shi, M. Hong, and B. Champagne, "Joint transceiver designs for full-duplex K-pair MIMO interference channel with SWIPT," *IEEE Trans. Commun.*, vol. 65, no. 2, pp. 890–905, Feb. 2017.

[44] M. M. Zhao, Q. Shi, Y. Cai, and M. J. Zhao, "Joint transceiver design for full-duplex cloud radio access networks with SWIPT," *IEEE Trans. Wireless Commun.*, vol. 16, no. 9, pp. 5644–5658, Sep. 2017.

[45] S. Boyd and L. Vandenberghe, *Convex Optimization*. Cambridge, U.K.: Cambridge Univ. Press, 2004.

[46] S. Boyd, L. Xiao, A. Mutapcic, and J. Mattingley, "Notes on decomposition methods," *Notes for EE364B, Stanford University*, pp. 1–36, 2007.

[47] M. Hong, M. Razaviyayn, Z. Luo, and J. Pang, "A unified algorithmic framework for block-structured optimization involving big data: With applications in machine learning and signal processing," *IEEE Signal Process. Mag.*, vol. 33, no. 1, pp. 57–77, Jan. 2016.

[48] C. Chen, B. He, Y. Ye, and X. Yuan, "The direct extension of ADMM for multi-block convex minimization problems is not necessarily convergent," *Math. Program.*, vol. 155, pp. 57–79, 2016.

[49] D. P. Bertsekas and J. N. Tsitsiklis, *Parallel and Distributed Computation: Numerical Methods*. USA: Prentice-Hall, Inc., 1989.

[50] K. E. Atkinson, *An introduction to numerical analysis*. John wiley & sons, 2008.